Three-dimensional failure criteria for fiber-reinforced laminates

G. Catalanotti [a,*], P.P. Camanho [a], A.T. Marques [a]

[a] *DEMec, Faculdade de Engenharia, Universidade do Porto, Rua Dr. Roberto Frias, 4200-465, Porto, Portugal*

Abstract

This paper proposes a new fully three-dimensional failure criteria for polymer composites reinforced by unidirectional fibers. Existing failure criteria based on three-dimensional stress states are revisited and their limitations and pitfalls are identified. A new set of failure criteria for both longitudinal and transverse failure mechanisms where the effect of ply thickness on the material strength is accounted for is proposed. The accuracy of the failure criteria is assessed by comparing the analytical predictions with existing experimental data obtained under multiaxial stress states. A good agreement between the the predictions and experimental data is generally observed.

Key words: A. Polymer-matrix composites (PMCs), B. Failure criteria

1 Introduction

The prediction of the onset of the failure mechanisms of the elementary ply in polymer composites reinforced by unidirectional fibers has been the subject of detailed investigations over the last twenty years [1–12]. In simple terms, the ply failure mechanisms may be divided into transverse failure mechanisms, which include cracking of both the matrix and fiber-matrix interface, and longitudinal failure mechanisms where cracking occurs in both the fibers and matrix.

While significant effort has been devoted to the prediction of ply failure mechanisms under plane stress states [3,4], more general failure criteria applicable

* Corresponding author
Email address: giuseppe.catalanotti@fe.up.pt (G. Catalanotti).

to general stress states are required [13]. Three-dimensional stress states occur not only at geometric discontinuities of multidirectional laminates (e.g. free-edges, open and loaded holes), but also in a number of relevant applications of composite materials such as raisers for oil extraction in deep waters. In addition, some of the recent developments in computational damage mechanics models for composite laminates [14,15] that simulate the propagation of ply failure mechanisms rely not only on the accurate prediction of the onset of failure but also on geometric information on the failure mechanism: the fracture plane.

Based on the previous observations, the main objective of this paper is to propose and to validate a new three-dimensional failure criteria for polymer composites that predicts the onset of the different failure mechanisms and that provides additional information on the type of failure and on the orientation of the fracture plane. The paper starts with a critical examination of existing three-dimensional failure criteria where some limitations and pitfalls are identified by applying the existing criteria under simple stress states. Next, the new failure criteria for longitudinal and transverse failure mechanisms are described and validated using both simple stress states and previously obtained experimental data results. Finally, the paper presents the main conclusions of this study and suggestions for future research.

2 Criteria for transverse failure mechanisms

In the following, some three-dimensional failure criteria for transverse, matrix-dominated failure mechanisms are critically revisited. According to Puck, the failure index for a general stress state is a scalar function of the traction vector acting on the fracture plane as shown in Figure 1. Defining α as the angle between the fracture plane and the through-the-thickness direction, the failure index depends on the tractions acting on the fracture surface and, therefore, on the angle α.

[Fig. 1 about here.]

Defining the unit normal vector to the fracture plane as:

$$\boldsymbol{n}_2 = \left\{ 0 \ \cos\left(\alpha\right) \ \sin\left(\alpha\right) \right\}^{\mathrm{T}} \tag{1}$$

the traction acting on the fracture plane, $\boldsymbol{t}$, is:

$$\boldsymbol{t} = \boldsymbol{\sigma} \cdot \boldsymbol{n}_2 \tag{2}$$

where $\boldsymbol{\sigma}$ is the stress tensor.

The orientation of the fracture plane is a function of the components of the traction vector that maximizes a failure index for a particular value of α. These components are the normal stress and the two shear stresses (longitudinal and transverse) as shown in Figure 1.

The normal, t_N, and the shear components, t_L and t_T, of the traction tensor are given as:

$$t_N = \boldsymbol{t} \cdot \boldsymbol{n}_2,\ t_L = \boldsymbol{t} \cdot \boldsymbol{n}_1,\ t_T = \boldsymbol{t} \cdot (\boldsymbol{n}_1 \times \boldsymbol{n}_2) \tag{3}$$

where $\boldsymbol{n}_1 = \left\{ 1\ 0\ 0 \right\}^{\mathrm{T}}$.

The failure criteria depends on the sign of the normal stress. There is a failure criterion for matrix compression if $t_N < 0$, and failure criterion for matrix tension when $t_N > 0$.

2.1 Overview of existing failure criteria for transverse compression

2.1.1 Puck's criterion

Puck *et al.* [16,17,5,9] performed matrix compression tests and observed that a modified Mohr-Coulomb criterion can be used to predict the orientation of the fracture plane. For pure transverse compression loading ($\sigma_{22} \neq 0$ and $\sigma_{ij} = 0$) the maximum shear stress occurs for $\alpha = \pm\pi/4$. However, experimentally it was observed that for fiber reinforced plastics the fracture angle is equal to $\alpha_0 = 53 \pm 2^\circ$ [16,17]. The difference between the two angles was associated with the effect of the compressive stress on the ply failure mechanisms.

Puck and Shürmann's criterion [5] is expressed as:

$$\phi_{MC} = \left(\frac{t_L}{S_L - \eta_L t_N} \right)^2 + \left(\frac{t_T}{S_T - \eta_T t_N} \right)^2 \tag{4}$$

This criterion does not account for the *in-situ* effects, i.e., for the increase of the shear strength of a ply when embedded in a multidirectional laminate [30]. Therefore the following modification of Puck's criterion is proposed:

$$\phi_{MC} = \left(\frac{t_L}{S_L^{is} - \eta_L t_N} \right)^2 + \left(\frac{t_T}{S_T^{is} - \eta_T t_N} \right)^2 \tag{5}$$

where S_L^{is} is the *in-situ* longitudinal shear strength, S_T^{is} is the *in-situ* transversal shear strength, and η_L and η_T are friction coefficients that correspond to the two slopes in the t_N-τ diagram when $t_N = 0$ and are defined as:

$$\eta_L = -\left.\frac{\partial t_L}{\partial t_N}\right|_{t_N=0} \qquad \eta_T = -\left.\frac{\partial t_T}{\partial t_N}\right|_{t_N=0} \tag{6}$$

It should be noted that the Fracture Mechanics models developed to estimate the in-situ strengths neglect the effect of the stiffness of the sub-laminates that constrain the ply. The values of the in-situ strengths accounting for the stiffness of the outer layers could be calculated using non-linear finite element methods with enough resolution through the thickness of the ply. Therefore, the values of the in-situ strengths used in this paper are, in general, approximate values of the strength of a ply.

Equation (5) can be used to evaluate in a consistent way the different parameters that define the failure criteria. The predictive capabilities of the criterion will be assessed in the following points by applying the criterion to simple stress states.

2.1.1.1 Hypothesis 1: $\sigma_{22} = -Y_C^{is}$ If only a compressive stress $\sigma_{22} = -Y_C^{is}$ is applied the material must fail with a fracture angle α equal to α_0.

Under pure transverse compression the failure index is expressed as:

$$\phi_{MC} = \frac{\sin^2(\alpha)\cos^2(\alpha)\,{Y_C^{is}}^2}{\left(S_T^{is} + \eta_T \cos^2(\alpha)\, Y_C^{is}\right)^2} \tag{7}$$

The derivative of (7) with respect to α yields:

$$\begin{aligned}\frac{\partial \phi_{MC}}{\partial \alpha} =& 2\,\frac{\sin(\alpha)\cos^3(\alpha)\,{Y_C^{is}}^2}{\left(S_T^{is} + \eta_T\,\cos(\alpha)^2\,Y_C^{is}\right)^2} - 2\,\frac{\sin^3(\alpha)\cos(\alpha)\,{Y_C^{is}}^2}{\left(S_T^{is} + \eta_T\,\cos^2(\alpha)\,Y_C^{is}\right)^2} \\ &+ 4\,\frac{\sin^3(\alpha)\cos^3(\alpha)\,{Y_C^{is}}^3\eta_T}{\left(S_T^{is} + \eta_T\,\cos^2(\alpha)\,Y_C^{is}\right)^3}\end{aligned} \tag{8}$$

Fracture must occur at the plane defined by the angles $\alpha = \alpha_0$ or $\alpha = \pi - \alpha_0$. For this value of α, the following conditions must apply: $\phi_{MC} = 1$ and $\partial\phi_{MC}/\partial\alpha = 0$. Substituting $\alpha = \alpha_0$ in equations (7) and (8), the transverse shear strength and the compressive transverse strength can be obtained solving the following system of non-linear equations:

$$\begin{cases} \phi_{MC}|_{\alpha=\alpha_0} = 1 \\ \frac{\partial \phi_{MC}}{\partial \alpha}\Big|_{\alpha=\alpha_0} = 0 \end{cases} \tag{9}$$

Assuming the relationship for the friction coefficients proposed by Puck and Shürmann [9]:

$$\eta_L/\eta_T = S_L^{is}/S_T^{is} \tag{10}$$

and considering that the in-plane shear strength and the longitudinal friction coefficient are material parameters that can be measured, the system of equations (9) is solved for Y_C^{is} and S_T^{is}:

$$Y_C^{is} = -\frac{S_L^{is}\left(2\cos^2(\alpha_0) - 1\right)}{\eta_L \cos^2(\alpha_0)} \tag{11}$$

$$S_T^{is} = \frac{1}{2}\frac{\left(2\sin^2(\alpha_0) - 1\right) S_L^{is}}{\sqrt{1-\sin^2(\alpha_0)}\sin(\alpha_0)\,\eta_L} \tag{12}$$

The longitudinal angle of internal friction, η_L, can be obtained from a 15° off-axis compression test [24]; the *in-situ* shear strength, S_L^{is}, is calculated from the analytical model proposed in [30].

If equations (11)-(12) are used, the failure index is equal to 1, the first derivative is equal to zero, and the second derivative reads:

$$\left.\frac{\partial^2 \phi_{MC}}{\partial \alpha^2}\right|_{\alpha=\alpha_0} = \frac{2}{\cos^2(\alpha_0)\left(\cos^2(\alpha_0) - 1\right)} \tag{13}$$

which is negative as required. If the conditions expressed by equations (11) and (12) are not satisfied, the function ϕ_{MC} will take the value 1 for $\alpha = \alpha_0$ but its maximum will not occurr for the correct fracture angle. This will result in errors if the failure angle is found maximizing numerically equation (7).

For example, for carbon IM7/8552 (S_L^{is}=130.2MPa, $\eta_L = 0.5$) the failure index as a function of the angle α is shown in Figure 2. It should be noticed that the maximum value of ϕ_{MC} is correctly calculated for $\alpha = \alpha_0$.

[Fig. 2 about here.]

2.1.1.2 Hypothesis 2: $\tau_{12} = S_L^{is}$ If only the shear stress $\tau_{12} = S_L^{is}$ is applied the fracture angle must be $\alpha = 0$.

In this case equation (5) results in:

$$\phi_{MC} = \cos^2(\alpha) \tag{14}$$

and:

$$\frac{\partial \phi_{MC}}{\partial \alpha} = -2\cos(\alpha)\sin(\alpha) \tag{15}$$

As expected, the failure index and the derivative are equal to 1 and 0 respectively when $\alpha = 0$. The second derivative of this function is negative ($\partial^2\phi_{MC}/\partial\alpha^2 = -2$) and this assures that the failure criterion is maximized. Figure 3 shows the failure index as a function of the angle α. The fracture angle is well predicted.

[Fig. 3 about here.]

2.1.1.3 Conclusion Puck's failure criterion describes very well the fracture of the matrix if the *in-situ* strengths Y_C^{is} and S_T^{is} are defined according to equations (11) and (12).

2.2 Overview of existing failure criteria for transverse tension

2.2.1 Quadratic Interaction Criterion

The quadratic interaction criterion proposed by Pinho [18] assumes a quadratic interaction between the components of the traction on the fracture plane. The criterion is given by the following expression:

$$\phi_{MT} = \left(\frac{t_N}{Y_T^{is}}\right)^2 + \left(\frac{t_L}{S_L^{is}}\right)^2 + \left(\frac{t_T}{S_T^{is}}\right)^2 \tag{16}$$

where Y_T^{is} is the *in-situ* transverse tensile strength. As before, Y_T^{is} is a function of the ply thickness, and it can be calculated using the equations derived in [30].

2.2.1.1 Hypothesis: $\sigma_{22} = Y_T^{is}$ Under this stress state the fracture plane should be $\alpha = 0$ and $\phi_{MT} = 1$. However, if the fracture angle is not known in advance, but rather searched by maximizing the failure index (equation (16)) with respect to α, which is the normal procedure in the computational implementation of the failure criterion, the failure index reads:

$$\phi_{MT} = \cos^4(\alpha) + \sin^2(\alpha)\cos^2(\alpha)\, k^2 \tag{17}$$

where $k = Y_T^{is}/S_T^{is}$.

Figure 4 shows ϕ_{MT} as a function of k and α.

[Fig. 4 about here.]

The derivative of equation (17) with respect to α is:

$$\frac{\partial \phi_{MT}}{\partial \alpha} = -4\,\cos^3(\alpha)\sin(\alpha) + 2\,\sin(\alpha)\cos^3(\alpha)\, k^2 - 2\,\sin^3(\alpha)\cos(\alpha)\, k^2 \tag{18}$$

while the second derivative of ϕ_{MT} with respect to α, for $\alpha = 0$ reads:

$$\left.\frac{\partial^2 \phi_{MT}}{\partial \alpha^2}\right|_{\alpha=0} = -4 + 2\,k^2 \tag{19}$$

which should be negative if $\alpha = 0$ maximizes the failure index, equation (17). Consequently in the case of a unidirectional tension the criterion provides correct predictions only if:

$$k \leq \sqrt{2}/2 \Rightarrow Y_T^{is} \leq \sqrt{2} S_T^{is} \tag{20}$$

For example, in the case of a thin ply of IM7/8552 carbon, $k = \frac{Y_T^{is}}{S_T^{is}} = 160.2/74.7 = 2.1$. It should be noted that the value of S_T^{is} is calculated using equation (12). The failure index ϕ_{MT} for IM7/8552 is reported in Figure 5.

[Fig. 5 about here.]

Figure 5 shows that under pure transverse tension, the failure criterion predicts that failure occurs when $\sigma_{22} < Y_T^{is}$, and the corresponding fracture plane is different than $\alpha = 0$. This is obviously wrong.

2.2.2 Mohr-Coulomb Criterion for Tension and Compression

Gutkin *et al* [31] use, for tension and compression, a modification of Puck's criterion (on (4)):

$$\phi_M = \left(\frac{t_L}{S_L - \eta_L t_N}\right)^2 + \left(\frac{t_T}{S_T - \eta_T t_N}\right)^2 + \left\langle \frac{t_N}{Y_T^{is}} \right\rangle \tag{21}$$

where $\langle \bullet \rangle$ is the McAuley operator defined as $\langle x \rangle = 1/2(x + |x|)$.

2.2.2.1 Hypothesis: $\sigma_{22} = Y_T^{is}$ Under this stress state the failure index reads:

$$\phi_{MT} = \phi_M|_{t_N=0} = \cos^2(\alpha) + \left(\frac{\sin(\alpha)\cos(\alpha)\, Y_T^{is}}{S_T^{is} - \eta_T \cos^2(\alpha)\, Y_T^{is}}\right)^2 \tag{22}$$

To be consistent with the experimental observations, the fracture angle must be located at $\alpha = 0$. This implies the following equations:

$$\left.\frac{\partial \phi_{MT}}{\partial \alpha}\right|_{\alpha=0} = 0 \tag{23}$$

$$\left.\frac{\partial^2 \phi_{MT}}{\partial \alpha^2}\right|_{\alpha=0} = -2 + 2\left(\frac{Y_T^{is}}{S_T^{is} - \eta_T Y_T^{is}}\right)^2 < 0 \tag{24}$$

Equation (24) results in:

$$-1 < \frac{Y_T^{is}}{S_T^{is} - \eta_T Y_T^{is}} < 1 \tag{25}$$

that it is not always respected in structural composites. For example, in the case of a thin ply of IM7/8552 carbon-epoxy ($Y_T^{is} = 160.2$, $S_T^{is} = 74.7$, $\eta_T = 0.3$), $\frac{Y_T^{is}}{S_T^{is} - \eta_T Y_T^{is}} = 6.0$; in this case equation (25) is not satisfied.

For this reason, under pure transverse tension, the failure criterion predicts that failure occurs when $\sigma_{22} < Y_T^{is}$, and the corresponding fracture plane is different than $\alpha = 0$.

2.2.3 Puck's criterion

Puck proposed the following elliptical interaction criterion [19]:

$$\phi_{MT} = \left(\frac{\tau}{S^{is}}\right)^2 + c_1 \frac{t_N}{Y_T^{is}} + c_2 \left(\frac{t_N}{Y_T^{is}}\right)^2 \tag{26}$$

where τ is the shear stress acting on the fracture plane, t_N is the normal stress and c_1 and c_2 are parameters that can be determined imposing appropriate boundary conditions. S^{is} is the shear strength on the fracture plane. The shear on the fracture plane is given as:

$$\tau = \sqrt{t_L^2 + t_T^2} \tag{27}$$

and the angle ω between the shear stress t_T and τ is equal to:

$$\omega = \arctan\left(t_L / t_T\right) \tag{28}$$

2.2.3.1 Determination of S^{is} If only t_T and t_L are non-zero, the failure criterion for tension (equation (26)) and for compression (equation (5)) should give the same results. Therefore, $\phi_{MC} = \phi_{MT}$ when $t_N = 0$.

Under this hypothesis the following expression for S^{is} is derived:

$$S^{is} = \left((\sin(\omega)/S_L^{is})^2 + (\cos(\omega)/S_T^{is})^2\right)^{-\frac{1}{2}} \tag{29}$$

2.2.3.2 Determination of c_1 and c_2 To calculate c_1 and c_2, consider a unidirectional tensile stress $\sigma_{22} = Y_T^{is}$ applied in the transverse direction. The failure index is equal to 1 and the fracture angle α is equal to 0. Imposing these conditions in equation (26) results in:

$$c_1 + c_2 = 1 \tag{30}$$

At failure ($\phi_{MT} = 1$) the shear stress τ can be obtained from equation (26) as a function of t_N ($\tau = \tau(t_n)$). The derivative of (26) with respect to the normal stress reads:

$$\frac{\partial \phi_{MT}}{\partial t_N} = \frac{2\tau}{{S^{is}}^2} \frac{\partial \tau}{\partial t_N} + \frac{c_1}{Y_T^{is}} + \frac{2c_2\, t_N}{{Y_T^{is}}^2} \tag{31}$$

Supposing now that $t_N = 0$, equation (31) results in:

$$\left.\frac{\partial \phi_{MT}}{\partial t_N}\right|_{t_N=0} = -\frac{2\tau\,\eta}{S^{is\,2}} + \frac{c_1}{Y_T^{is}} \tag{32}$$

whit $\eta = -\left.\frac{\partial \tau}{\partial t_N}\right|_{t_N=0}$.

The parameter η can be expressed in function of η_L and η_T. Considering the following equation:

$$\tau^2 = t_L^2 + t_T^2 \tag{33}$$

and differentiating it with respect to the normal stress results:

$$2\tau\frac{\partial \tau}{\partial t_N} = 2t_L\frac{\partial t_L}{\partial t_N} + 2t_T\frac{\partial t_T}{\partial t_N} \tag{34}$$

Using the definition of the friction coefficients (equation (6)), under the hypothesis of $t_N = 0$, equation (34) yields:

$$\eta = \eta_L\ t_L/\tau + \eta_T\ t_T/\tau \tag{35}$$

To calculate the coefficient c_1, consider the following stress state: $t_N = 0$, $t_T = 0$ and $t_L = S_L^{is}$. In this case the matrix should fail and the derivative of equation (32) should be equal to zero because the failure index is a maximum. Under these hypotheses $\eta|_{t_T=0} = \eta_L$ and equation (32) can be re-written as:

$$\frac{\partial \phi_{MT}}{\partial t_N} = -\frac{2\eta_L}{S_L^{is}} + \frac{c_1}{Y_T^{is}} = 0 \quad \Longrightarrow c_1 = \frac{2\eta_L Y_T^{is}}{S_L^{is}} \tag{36}$$

Substituting the c_1 in equation (30) c_2 is obtained:

$$c_1 + c_2 = 1 \quad \Longrightarrow c_2 = 1 - 2\,\eta_L Y_T^{is}/S_L^{is} \tag{37}$$

Therefore, the failure index given by equation (26) results in:

$$\phi_{MT} = \left(\frac{\tau}{S^{is}}\right)^2 + \frac{2\eta_L t_N}{S_L^{is}} + \left(1 - \frac{2\eta_L Y_T^{is}}{S_L^{is}}\right)\left(\frac{t_N}{Y_T^{is}}\right)^2 \tag{38}$$

2.2.3.3 Hypothesis: $\sigma_{22} = Y_T^{is}$. If $\sigma_{22} = Y_T^{is}$ with $\sigma_{ij} = 0$ the material must fail by transverse matrix cracking and the angle should be $\alpha = 0$. The

failure index under this hypothesis is $\phi_{MT} = 1$ and the first derivative is equal to $\partial\phi_{MT}/\partial\alpha = 0$.

The second derivative of ϕ_{MT} reads:

$$\left.\frac{\partial^2\phi_{MT}}{\partial\alpha^2}\right|_{\alpha=0} = \frac{2{Y_T^{is}}^2}{{S_T^{is}}^2} - \frac{4\eta_L Y_T^{is}}{S_L^{is}} - \frac{4\left(S_L^{is} - 2\eta_L Y_T^{is}\right)}{S_L^{is}} \tag{39}$$

that should be negative if the fracture angle α corresponds to the maximum of ϕ_{MT}. The second derivative is negative when:

$$\frac{\left(-\eta_L S_T^{is} + \sqrt{{\eta_L}^2{S_T^{is}}^2 + 2{S_L^{is}}^2}\right) S_T^{is}}{S_L^{is}} < Y_T^{is} < \frac{\left(-\eta_L S_T^{is} - \sqrt{{\eta_L}^2{S_T^{is}}^2 + 2{S_L^{is}}^2}\right) S_T^{is}}{S_L^{is}} \tag{40}$$

For example, for carbon IM7/8552 equation (40) can be written as:

$$-129 < Y_T^{is} < 86 \quad \text{[MPa]} \tag{41}$$

This means that in this case, for $\alpha = 0$, ϕ_{MT} will not be a maximum. This is clearly shown in Figure 6 that represents ϕ_{MT} as a function of α.

[Fig. 6 about here.]

2.2.4 Proposed Failure Criterion

The three-dimensional interaction criteria previously described cannot be used to predict the failure of the matrix under general stress states because, for the case of a simple transverse compression, they provide reasonable predictions only if some relations between the material strengths are satisfied. These relations are not realistic for most structural composites where *in-situ* effects are accounted for. Therefore, a new failure criterion is proposed here.

As previously shown, the failure criteria available in literature cannot be used to predict failure when transverse tension σ_{22} (or σ_{33}) is applied. In that case there is a combination of t_N and t_T on the generic fracture plane and, citing [19], "*if the resistance of the action plane against t_T shear fracture would be considerably smaller than that against transverse tension a different fracture angle $\alpha = 0$ would occur*".

In other words, when transverse tension is applied, the fracture angle for $\alpha \neq 0$ will be function of Y_T^{is} and S_T^{is} and, consequently, it will depend on the material system.

Therefore, it is appropriate to propose the following failure criterion for transverse matrix cracking:

$$\phi_{MT} = \left(\frac{t_N}{S_T^{is}}\right)^2 + \left(\frac{t_L}{S_L^{is}}\right)^2 + \left(\frac{t_T}{S_T^{is}}\right)^2 + \lambda \left(\frac{t_N}{S_T^{is}}\right)\left(\frac{t_L}{S_L^{is}}\right)^2 + \kappa \left(\frac{t_N}{S_T^{is}}\right) \tag{42}$$

where t_N, t_T and t_L are defined in equation (3).

It should be noted that the failure index proposed satisfy the following conditions:

- $\phi_{MT} = 1$ when $t_T = S_T^{is}$ and $\sigma_{ij} = 0$;
- $\phi_{MT} = 1$ when $t_L = S_L^{is}$ and $\sigma_{ij} = 0$;
- $\phi_{MT} = \phi_{MC}$ when $t_N = 0$. In this case $\phi_{MT} = \phi_{MC} = (t_T/S_T^{is})^2 + (t_L/S_L^{is})^2$.

The parameter κ is determined imposing that $\phi_{MT} = 1$ when $t_N = Y_T^{is}$. It reads:

$$\kappa = \frac{S_T^{is\,2} - Y_T^{is\,2}}{S_T^{is} Y_T^{is}} \tag{43}$$

The parameter λ is determined imposing that the failure indices for transverse tension and compression should have continuous first derivative when $t_N = 0$. At failure ($\phi_{MT} = 1$), the shear stress t_L reads:

$$t_L = \frac{\sqrt{S_T^{is}\ (S_T^{is} + \lambda\, t_N)\left(-{t_N}^2 - \kappa\, t_N\, S_T^{is} + {S_T^{is}}^2\right)}\, S_L^{is}}{S_T^{is}\ (S_T^{is} + \lambda\, t_N)} \tag{44}$$

Taking the limit for $t_N \to 0$ of the derivative of equation (44) and imposing that for both tension and compression $\left.\frac{\partial t_L}{\partial t_N}\right|_{t_N=0} = -\eta_L$, the following equation is obtained:

$$\lambda = 2\,\eta_L S_T^{is}/S_L^{is} - \kappa \tag{45}$$

In the following it will be shown that the proposed failure criterion is able to predict both the fracture plane and the strength. The following stress states are considered:

- transverse tensile stress ($\sigma_{22} = Y_T^{is}$, $\sigma_{33} = Y_T^{is}$);
- longitudinal shear stress ($\tau_{12} = S_L^{is}$,$\tau_{13} = S_L^{is}$);

- transverse shear stress ($\tau_{23} = \tau_{23}^{crit}$).

2.2.4.1 Hypothesis 1 Considering $\sigma_{22} = Y_T^{is}$ the function ϕ_{MT} reads:

$$\phi_{MT} = \cos^2(\alpha) \tag{46}$$

Figure 7 shows ϕ_{MT} as a function of α. The predicted fracture plane is correctly computed as $\alpha = 0$ and $\phi_{MT} = 1$.

[Fig. 7 about here.]

2.2.4.2 Hypothesis 2 Considering $\sigma_{33} = Y_T^{is}$ the function ϕ_{MT} takes the value:

$$\phi_{MT} = \sin^2(\alpha) \tag{47}$$

Figure 8 shows ϕ_{MT} as a function of α. The predicted fracture plane is correctly computed as $\alpha = \pi/2$. The failure index is $\phi_{MT} = 1$ at the fracture plane.

[Fig. 8 about here.]

2.2.4.3 Hypothesis 3 Considering $\tau_{12} = S_L^{is}$ the function ϕ_{MT} reads:

$$\phi_{MT} = \cos^2(\alpha) \tag{48}$$

Figure 9 shows ϕ_{MT} as a function of α. The predicted fracture plane is correctly computed as $\alpha = 0$ and the failure index $\phi_{MT} = 1$.

[Fig. 9 about here.]

2.2.4.4 Hypothesis 4 Considering $\tau_{13} = S_L^{is}$ the function ϕ_{MT} reads:

$$\phi_{MT} = \sin^2(\alpha) \tag{49}$$

Figure 10 shows ϕ_{MT} as a function of α. The predicted fracture plane is correctly computed, $\alpha = \pi/2$, and $\phi_{MT} = 1$.

[Fig. 10 about here.]

2.2.4.5 Hypothesis 5: $\tau_{23} = \tau_{23}^{crit}$ Assuming, without loss of generality that $\tau_{23}^{crit} > 0$. The normal stress (equation (3)) yields:

$$\begin{array}{lll} t_N > 0 & \text{if} & 0 < \alpha < \pi/2 \\ t_N = 0 & \text{if} & \alpha = \pi/2 \\ t_N < 0 & \text{if} & \pi/2 < \alpha < \pi \end{array} \tag{50}$$

Consequently, the failure index, ϕ_M reads:

$$\phi_M = \begin{cases} \frac{{\tau_{23}^{crit}}^2 {Y_T^{is}} + \tau_{23}^{crit} {S_T^{is}}^2 \sin(2\,\alpha) - \tau_{23}^{crit} {Y_T^{is}}^2 \sin(2\,\alpha)}{{S_T^{is}}^2 Y_T^{is}} & \text{if} \quad 0 < \alpha < \pi/2 \\ \frac{{\tau_{23}^{crit}}^2 (\sin(\alpha) - \cos(\alpha))^2 (\sin(\alpha) + \cos(\alpha))^2}{\left(-S_T^{is} + 2\,\eta_T\, \cos(\alpha) \sin(\alpha) \tau_{23}^{crit}\right)^2} & \text{if} \quad \pi/2 < \alpha < \pi \end{cases} \tag{51}$$

If τ_{23} is the only non-zero stress, there are three action planes on which only one component of the stress tensor acts:

- on $\alpha = 0$ and $\alpha = \pi/2$ only t_T is acting;
- on $\alpha = \pi/4$ only t_N (that corresponds to the principal tensile stress σ_I) is acting.

These stresses (see figure 11) are all in magnitude equal to τ_{23}. That means that if $Y_T^{is} > S_T^{is}$ (S_T^{is} is the critical value) the fracture planes will be $\alpha = 0$ and $\alpha = \pi/2$, while if $S_T^{is} > Y_T^{is}$ (Y_T^{is} is the critical value) the fracture plane will be $\alpha = \pi/4$.

[Fig. 11 about here.]

case 1: $Y_T^{is} > S_T^{is}$

If S_T^{is} is the critical value, the failure index of equation (51) reads:

$$\phi_M = \begin{cases} \frac{-2\, \sin(\alpha) \cos(\alpha) {Y_T^{is}}^2 + 2\, \sin(\alpha) \cos(\alpha) {S_T^{is}}^2 + S_T^{is}\, Y_T^{is}}{S_T^{is}\, Y_T^{is}} & \text{if} \quad 0 < \alpha < \pi/2 \\ -\frac{4\, \cos^4(\alpha) - 4\, \cos^2(\alpha) + 1}{-1 + 4\,\eta_T\, \cos(\alpha) \sin(\alpha) - 4\,{\eta_T}^2 \cos^2(\alpha) + 4\,{\eta_T}^2 \cos^4(\alpha)} & \text{if} \quad \pi/2 < \alpha < \pi \end{cases} \tag{52}$$

Figure 12 shows ϕ_M as a function of α. The predicted fracture planes are correctly computed as $\alpha = 0,\ \pi/2$ and the failure index takes in these points the value of $\phi_M = 1$.

[Fig. 12 about here.]

case 2: $S_T^{is} > Y_T^{is}$

If Y_T^{is} is the critical value, the failure index of equation (51) reads:

$$\phi_M = \begin{cases} \frac{-2\,\sin(\alpha)\cos(\alpha)\,{Y_T^{is}}^2 + 2\,\sin(\alpha)\cos(\alpha){S_T^{is}}^2 + {Y_T^{is}}^2}{{S_T^{is}}^2} & \text{if} \quad 0 < \alpha < \pi/2 \\ \frac{-{Y_T^{is}}^2\cos(4\,\alpha) - {Y_T^{is}}^2}{-2\,{S_T^{is}}^2 + 4\,S_T^{is}\,\eta_T\,Y_T^{is}\,\sin(2\,\alpha) - \eta T^2\,{Y_T^{is}}^2 + {\eta_T}^2\,{Y_T^{is}}^2\cos(4\,\alpha)} & \text{if} \quad \pi/2 < \alpha < \pi \end{cases} \tag{53}$$

Figure 13 shows ϕ_M as a function of α. The predicted fracture plane is correctly computed as $\alpha = \pi/4$ and the failure index takes in these points the value of $\phi_M = 1$.

[Fig. 13 about here.]

2.2.4.6 Summary The criterion defined provides feasible predictions for the different load cases analyses. In summary:

- if $\sigma_{22} = Y_T^{is}$ and $\sigma_{ij} = 0$ the fracture plane is $\alpha = 0$;
- if $\sigma_{33} = Y_T^{is}$ and $\sigma_{ij} = 0$ the fracture plane is $\alpha = \pi/2$;
- if $\tau_{12} = S_L^{is}$ and $\sigma_{ij} = 0$ the fracture plane is $\alpha = 0$;
- if $\tau_{13} = S_L^{is}$ and $\sigma_{ij} = 0$ the fracture plane is $\alpha = \pi/2$;
- if $\tau_{23} = \tau_{23}^{crit}$ and $\sigma_{ij} = 0$:
  - if $\tau_{23}^{crit} = S_T^{is}$ the fracture plane is $\alpha = 0,\ \pi/2$;
  - if $\tau_{23}^{crit} = Y_T^{is}$ the fracture plane is $\alpha = \pi/4$;

3 Criteria for longitudinal failure mechanisms

3.1 Longitudinal tension failure ($\sigma_{11} > 0$)

The function that predicts longitudinal tensile fracture is the maximum strain criterion:

$$\phi_{LT} = \varepsilon_{11}/\varepsilon_1^T \tag{54}$$

3.2 Longitudinal kinking failure ($\sigma_{11} \leq 0$)

The three-dimensional stress states have relevant effects on the fiber kinking failure mode. Two hypotheses for the mechanic of fiber kinking are normally put forward:

- the first hypothesis, from Rosen, considers that kink bands are the final result of micro-buckling of the fibers [20];
- the second hypothesis, from Argon, assumes that kink bands are triggered by localized matrix failure in the vicinity of misaligned fibers [21].

Schultheisz and Waas [22] concluded that in structural composites kinking is originated by local micro-structural defects that could trigger the kinking phenomenon. The model proposed here is based on Argon's hypothesis [21] and on the subsequent developments by Dávila *et al.* [12] and Pinho *et al.* [18].

Figure 14 shows the different coordinate systems and planes that are used in the model. The coordinate system 123 is aligned with the material axes of the composite: 1 represents the fiber direction, 2 and 3 the transverse directions.

The kinking plane is shown in Figure 14(a). The coordinate system associated to the kinking plane is $1^{(\theta)}2^{(\theta)}3^{(\theta)}$ and it is obtained by the rotation of the frame 123 around the axis 1 of an angle θ.

Figure 14(b) show the fibers on the kinking plane. The kinking-angle is φ and the respective coordinate system is $1^{(\varphi)}2^{(\varphi)}3^{(\varphi)}$ that can be obtained by $1^{(\theta)}2^{(\theta)}3^{(\theta)}$ after a rotation of an angle φ around the axis $3^{(\theta)}$. After this transformation it is possible to use the failure criteria, equations (5) and (42), in the misalignment coordinate system $1^{(\varphi)}2^{(\varphi)}3^{(\varphi)}$ to predict fiber kinking.

Figure 14(c) shows the fracture angle with respect to the misalignment frame, and identified by the angle α.

[Fig. 14 about here.]

Kinking failure can then be predicted using the matrix failure index in the misalignment frame. This requires two rotations of the stress tensor.

We assume that the angle θ is a function of the stresses state. Supposing that the kinking plane is defined by the shear stress that act on the 2-3 plane (see Figure 15), the angle θ can be calculated as:

$$\theta = \arctan\left(\tau_{13}/\tau_{12}\right) \tag{55}$$

If both τ_{12} and τ_{13} are equal to zero the kinking angle can be calculated by the maximum principal stress that acts on the transversly isotropic plane. In fact, if $\tau_{23}^{(\theta)} \neq 0$ this will result in a movement perpendicular to the kinking-plane contradicting the evidence that fibers kink on this plane [18]. The angle θ can be obtained as:

$$\theta = \frac{1}{2}\arctan\left(\frac{2\tau_{23}}{\sigma_{22}-\sigma_{33}}\right) \tag{56}$$

[Fig. 15 about here.]

If a rotation of θ (counterclockwise) is applied the stress tensor in the new coordinate system results $\boldsymbol{\sigma}^{(\theta)} = \boldsymbol{R}^{(\theta)} \cdot \boldsymbol{\sigma} \cdot \boldsymbol{R}^{(\theta)^T}$ where $\boldsymbol{R}^{(\theta)}$ is the rotation matrix defined as:

$$\boldsymbol{R}^{(\theta)} = \begin{bmatrix} 1 & 0 & 0 \\ 0 & \cos(\theta) & \sin(\theta) \\ 0 & -\sin(\theta) & \cos(\theta) \end{bmatrix} \tag{57}$$

Having found the fiber-kinking plane, the stresses should be rotated to the misalignment frame. The stresses on this coordinate system can be written as: $\boldsymbol{\sigma}^{(\varphi)} = \boldsymbol{R}^{(\varphi)} \cdot \boldsymbol{\sigma}^{(\theta)} \cdot \boldsymbol{R}^{(\varphi)^T}$ where $\boldsymbol{R}^{(\varphi)}$ is the rotation matrix defined as:

$$\boldsymbol{R}^{(\varphi)} = \begin{bmatrix} \cos(\varphi) & \sin(\varphi) & 0 \\ -\sin(\varphi) & \cos(\varphi) & 0 \\ 0 & 0 & 1 \end{bmatrix} \tag{58}$$

Having defined the stress in the misalignment frame, the matrix failure mode that triggers fiber kinking is predicted using equations (5) and (42). The components of the traction on the fracture plane can be expressed as:

$$t_N^{(\varphi)} = \cos^2(\alpha)\,\sigma_{22}^{(\varphi)} + 2\cos(\alpha)\sin(\alpha)\,\tau_{23}^{(\varphi)} + \sin^2(\alpha)\,\sigma_{33}^{(\varphi)} \tag{59}$$

$$t_T^{(\varphi)} = -\sin(\alpha)\cos(\alpha)\left(\sigma_{22}^{(\varphi)} - \sigma_{33}^{(\varphi)}\right) + \left(\cos^2(\alpha) - \sin^2(\alpha)\right)\tau_{23}^{(\varphi)} \tag{60}$$

$$t_L^{(\varphi)} = \cos(\alpha)\,\tau_{12}^{(\varphi)} + \sin(\alpha)\,\tau_{13}^{(\varphi)} \tag{61}$$

If $t_N^{(\varphi)} < 0$ the failure index becomes:

$$\phi_{KMC} = \left(\frac{t_L^{(\varphi)}}{S_L^{is} - \eta_L t_N^{(\varphi)}} \right)^2 + \left(\frac{t_T^{(\varphi)}}{S_T^{is} - \eta_T t_N^{(\varphi)}} \right)^2 \tag{62}$$

while if $t_N^{(\varphi)} \geq 0$ the failure index reads:

$$\phi_{KMT} = \left(\frac{t_N^{(\varphi)}}{S_T^{is}} \right)^2 + \left(\frac{t_L^{(\varphi)}}{S_L^{is}} \right)^2 + \left(\frac{t_T^{(\varphi)}}{S_T^{is}} \right)^2 + \lambda \left(\frac{t_N^{(\varphi)}}{S_T^{is}} \right) \left(\frac{t_L^{(\varphi)}}{S_L^{is}} \right)^2 + \kappa \left(\frac{t_N^{(\varphi)}}{S_T^{is}} \right) \tag{63}$$

where κ and λ are defined respectively in equations (43) and (45) .

The failure index for fiber kinking will take the value:

$$\phi_K = \max \left\{ \max \left\{ \phi_{KMC} \right\}, \max \left\{ \phi_{KMT} \right\} \right\} \tag{64}$$

where $\max \{\phi_{KMC}\}$ and $\max \{\phi_{KMT}\}$ are the maximum values of equations (62) and (63) with respect to α.

3.2.1 Determination of the angle φ

Dávila *et al.* [12] used a combination of Argon's approach and LaRC02/03 failure criterion to calculate the angle φ for plane stress states. The stresses in the misalignment coordinate frame of Figure 16 are:

$$\sigma_{11}^{(m)} = \cos^2(\varphi)\sigma_{11} + \sin^2(\varphi)\sigma_{22} + 2\sin(\varphi)\cos(\varphi)|\tau_{12}| \tag{65}$$
$$\sigma_{22}^{(m)} = \sin^2(\varphi)\sigma_{11} + \cos^2(\varphi)\sigma_{22} - 2\sin(\varphi)\cos(\varphi)|\tau_{12}| \tag{66}$$
$$\tau_{12}^{(m)} = \sin(\varphi)\cos(\varphi)(\sigma_{22} - \sigma_{11}) + \left(\cos^2(\varphi) - \sin^2(\varphi)\right)|\tau_{12}| \tag{67}$$

[Fig. 16 about here.]

Supposing that the material fails under axial compression the stresses take the values $\sigma_{11} = -X_C$, $\sigma_{22} = \tau_{12} = 0$. Substituting these values, equations (65) can be rewritten

$$\sigma_{11}^{(m)} = -\cos^2(\varphi_C) X_C \tag{68}$$
$$\sigma_{22}^{(m)} = -\sin^2(\varphi_C) X_C \tag{69}$$
$$\tau_{12}^{(m)} = \sin(\varphi_C)\cos(\varphi_C) X_C \tag{70}$$

where φ_C is the angle at the failure when a pure axial compression is applied.

Substituting these stresses in the LaRC02/03 failure criterion it becomes:

$$S_L^{is} = X_C \left(\sin(\varphi_C)\cos(\varphi_C) - \eta_L \sin^2(\varphi_C)\right) \tag{71}$$

Equation (71) can be solved for φ_C obtaining

$$\varphi_C = \arctan\left(\frac{1 - \sqrt{1 - 4\left(\frac{S_L^{is}}{X_C} + \eta_L\right)\frac{S_L^{is}}{X_C}}}{2\left(\frac{S_L^{is}}{X_C} + \eta_L\right)}\right) \tag{72}$$

The total misalignment φ is taken as the sum of an initial constant misalignment angle φ_0 (that represents the manufacture defects and imperfections in the materials) and a γ_m angle that is originated by the shear loading applied and depends on the shear constitutive law $\tau = f(\gamma_m)$.

At failure under axial compression the additional angle γ_m becomes:

$$\gamma_{mC} = f^{-1}\left(\tau_{12}^{(m)}\right) = f^{-1}\left(\sin(\varphi_C)\cos(\varphi_C) X_C\right) \tag{73}$$

For a material that exhibits linear behavior in shear, $\tau_{12}^{(m)} = G_{12}\gamma_m$ equation (73) can be solved in close form obtaining

$$\gamma_{mC} = \frac{\sin(2\varphi_C) X_C}{2G_{12}} \approx \frac{\varphi_C X_C}{G_{12}} \tag{74}$$

considering small angle approximation.

The initial misalignment angle can then obtained as:

$$\varphi_0 = \varphi_C - \gamma_{mC} \tag{75}$$

For a generic loading the strain γ_m is obtained solving the equation $f(\gamma_m) = \tau_{12}^{(m)}$ that can be written as:

$$f(\gamma_m) = -\sin(\varphi)\cos(\varphi)(\sigma_{11} - \sigma_{22}) + \left(\cos^2(\varphi) - \sin^2(\varphi)\right)|\tau_{12}| \tag{76}$$

Solving equation (76) for γ_m the angle φ becomes:

$$\varphi = \operatorname{sgn}\{\tau_{12}\}(\varphi_0 + \gamma_m) \tag{77}$$

Assuming small angle approximations, equation (76) yields:

$$f(\gamma_m) = (\varphi_0 + \gamma_m)(-\sigma_{11} + \sigma_{22}) + |\tau_{12}| \tag{78}$$

For a material that exhibits linear behavior the previous equation results in:

$$\gamma_m = \frac{\varphi_0 G_{12} + |\tau_{12}|}{G_{12} + \sigma_{11} - \sigma_{22}} - \varphi_0 \tag{79}$$

Pinho *et al.* [18] suggested to apply the the equations (76- 79) considering the stresses that acts on the kinking plane. Equation (76) becomes:

$$f(\gamma_m) = -\sin(\varphi)\cos(\varphi)\left(\sigma_{11}^{(\theta)} - \sigma_{22}^{(\theta)}\right) + \left(\cos^2(\varphi) - \sin^2(\varphi)\right)\left|\tau_{12}^{(\theta)}\right| \tag{80}$$

Finally for linear shear behavior equation (80) results:

$$\gamma_m = \frac{\varphi_0 G_{12} + \left|\tau_{12}^{(\theta)}\right|}{G_{12} + \sigma_{11}^{(\theta)} - \sigma_{22}^{(\theta)}} - \varphi_0 \tag{81}$$

3.2.2 Alternative determination of φ

The calculation of an initial misalignment angle, φ_0, causes an incompatibility between equations (5),(42) and (62),(63). Therefore, a new methodology for the calculation of the angle φ is proposed here.

The continuity of the failure envelope imposes that:

$$\phi_{KMC}|_{\sigma_{11}=0} = \phi_{MC} \tag{82}$$

$$\phi_{KMT}|_{\sigma_{11}=0} = \phi_{MT} \tag{83}$$

Equations (82) and (83) are verified only when the initial misalignment angle, φ_0, is equal to zero.

Substituting $\varphi_0 = 0$ in equation (75) results in:

$$\varphi_C = \gamma_{mC} \tag{84}$$

where the angle φ_C is computed in equation (72). To compute γ_{mC} equation (73) needs to be solved. For a material that exhibits a linear behavior in shear it can be assumed:

$$\tau_{12}^{(m)} = \chi \gamma_m \tag{85}$$

where χ is a micro-mechanical parameter associated with the creation of a kink-band.

The parameter χ can be obtained solving the equation (84):

$$\chi = \frac{\sin\left(2\,\varphi_C\right)\, X_C}{2\,\varphi_C} \tag{86}$$

For a generic loading the strain γ_m is obtained solving the equation (76). The angle φ becomes:

$$\varphi = \operatorname{sgn}\left\{\tau_{12}\right\} \gamma_m \tag{87}$$

Assuming small angle approximation, equation (76) can be expanded in a Taylor series and several expressions of γ_m can be found as functions of the boundary conditions.

This method is not feasible as a low-order Taylor series involving small angles is too approximate while a higher-order series leads to complicated expressions for γ_m; this will cause numerical instabilities in the calculation of γ_m.

It is easy and numerically more stable to solve equation (85) using, for example, the Newton-Raphson method. Equation (85), in fact, can be expressed as:

$$F = \chi\gamma_m + \frac{1}{2}\left(\sigma_{11} - \sigma_{22}\right)\sin\left(2\gamma_m\right) - \left|\tau_{12}\right|\cos\left(2\gamma_m\right) \tag{88}$$

and its derivative with respect to γ_m is:

$$\frac{\mathrm{d}F}{\mathrm{d}\gamma_m} = \chi + (\sigma_{11} - \sigma_{22})\cos(2\gamma_m) + 2\,|\tau_{12}|\sin(2\gamma_m) \tag{89}$$

The angle γ_m can be computed with the recursive formula:

$$\gamma_{mi+1} = \gamma_{mi} - \frac{F|_{\gamma_m=\gamma_{mi}}}{\left.\frac{\mathrm{d}F}{\mathrm{d}\gamma_m}\right|_{\gamma_m=\gamma_{mi}}} \tag{90}$$

4 Failure envelopes

The failure envelopes for several stress states are shown in Figures 17-19(c) for the IM7/8552 carbon laminate. The material properties used are shown in Table 1 [1] .

[Table 1 about here.]

[Fig. 17 about here.]

Figure 17(a) shows τ_{12} as a function of σ_{22}. As expected, when σ_{22} becomes compressive the apparent shear strength increases. It should be noticed that the envelope shows a continuity in the first derivative for $t_N = 0$.

Figure 17(b) shows τ_{13} as a function of σ_{22}. As τ_{13} and σ_{22} act on different planes no interaction between them is noticed and the value of τ_{13} remains always equal to or lower than S_L^{is}.

Figure 18(a) shows τ_{12} as a function of σ_{22} when the transverse stress, σ_{33}, is applied. The red envelopes are obtained when σ_{33} is positive and the blue ones when it is negative. If $\sigma_{33} > 0$ the envelope remain constant when $\sigma_{22} > 0$. This can be explained with the fact that there is no interaction between σ_{22} and σ_{33} when both are positive. In this case the fracture plane is calculated using the principal stress on the transverse plane (23). If $\sigma_{22} < 0$, an application of a positive σ_{33} decreases the strength. In the case that a compressive σ_{33} is applied the reduction of strength is noticed in tension ($\sigma_{22} > 0$) although in compression ($\sigma_{22} < 0$) the compressive σ_{33} is beneficial.

[1] It should be noted that *in-situ* strength are used; therefore, an embedded lamina is considered.

Figure 17(f) shows the σ_{11}-σ_{22} failure envelope where are highlighted the regions interested by different failure phenomena.

In the region characterized by kinking for matrix compression, the LaRC03 failure criterion predicts an increase of the apparent axial compressive strength and this is confirmed by experimental results [23]. The criterion proposed does not show an increase of the compressive strength if a biaxial compression is applied. This seems to contradict the experimental evidence but it is not the case. First of all, it should be noted that the fact that the compressive stress does not increase can be explained remembering the definition of the angle θ that identify the kink band plane. When σ_{22} becomes smaller than zero ($\sigma_{33} = 0$), the angle of the principal stress changes from 0° to 90°. If a compression in 2 direction is applied this will not influence the fiber kinking because the fiber will kink in the perpendicular plane. It is consistent with the model defined having a constant value of the compressive strength when $\sigma_{22} < 0$. However, if the loading condition or the manufacture of the material can justify a predisposition of the material to kink with an angle $\theta = 0$ (in 2 direction) the proposed failure criteria can detect the increasing of compressive strength in the biaxial compression region.

Figure 18(e) shows the σ_{11}-σ_{22} failure envelope when a transverse stress is applied.

In this case, if both σ_{22} and σ_{33} are compressive the increase of the strength in the biaxial compression region is shown. It should be noted that when transverse compression is applied ($\sigma_{33} < 0$) the strength of the material decreases in tension ($\sigma_{22} > 0$) and increases in compression ($\sigma_{22} < 0$). When transverse tension is applied the compressive strength decreases ($\sigma_{22} < 0$) but no effects are observed in the tensile strength ($\sigma_{22} > 0$). This is due to the fact that in tension ($\sigma_N > 0$,$\tau_L = 0$) the failure index is function of the principal stress on the transversal plane (23), it means that there is not interaction between σ_{22} and σ_{33} because the failure depends only on the maximum value of σ_{22} or σ_{33}. In this case in fact $\sigma_N = \max\{\sigma_{22}, \sigma_{33}\}$.

[Fig. 18 about here.]

Figure 19 shows the failures envelopes that relate σ_{33} with σ_{22} for different values of the shear stresses τ_{12}, τ_{13} and τ_{23}.

As expected, when the shear stresses (τ_{12}, τ_{13}, τ_{23}) are equal to zero the failure envelope intercept the two axis in the points $(Y_T, 0)$, $(0, Y_T)$, $(-Y_C, 0)$ and $(0, -Y_C)$. Moreover, when σ_{22} and σ_{33} are both positive the failure envelope remains correctly inside the region defined by $\sigma_{22} \leq 0$ and $\sigma_{33} \leq 0$. Finally, it is noted that the failure envelopes are open in the region characterized by hydrostatic pressure ($\sigma_{22} = \sigma_{33} = -p$).

It should pointed out that the fact that the σ_{22}-σ_{33} envelopes of Figure 19 are open in the region characterized by biaxial-compression does not mean that the material does not fail, but rather that Puck's criterion cannot predict failure. Experimentally, under high values of hydrostatic compression the resins used in structural composites exhibit yielding and the same should occur in an unidirectional lamina when biaxial compression is applied in the transverse plane (2-3). Presumably, if a yield criterion is used in combination to the proposed failure criteria, the envelopes should be closed in the region characterized by hydrostatic compression and should exhibit a more gradual variation in the region characterized by hydrostatic tension.

[Fig. 19 about here.]

5 Verification Problems

5.1 Example 1: Relationship between Y_C^{is}, η_L and S_L^{is}

In Section 2.1.1 the following relationship between Y_C^{is}, η_L and S_L^{is} was found:

$$Y_C^{is} = -\frac{S_L^{is}\left(2\cos^2\left(\alpha_0\right)-1\right)}{\eta_L \cos^2\left(\alpha_0\right)} \tag{91}$$

This relationship is written for the *in-situ* properties but has to be satisfied also in the case of a unidirectional lamina.

Equation (91) must be satisfied for the structural composites commonly used. Table 2 reports the material parameters of AS4/55A [27], E-Glass–LY556–HT907–DY063 [10] and T800–3900-2 [28] unidirectional laminae.

[Table 2 about here.]

Figure 20 shows the τ_{12} as a function of σ_{22} for the materials considered. It is observed that the transverse compressive stress is accurately predicted. This is further highlighted in Table 3 that reports the measured S_L, Y_C, η_L and the value of Y_C calculated using equation (91).

[Fig. 20 about here.]

[Table 3 about here.]

5.2 Example 2: σ_{22}-τ_{12} failure envelopes

Figure 21 show the σ_{22}-τ_{12} failure envelopes for four different materials: AS4/55A, E-Glass/LY556/HT907/DY063, T800/3900-2, AS4/3501-6 and IM7/8552. The material properties are reported in Tables 2, 4 and 5.

[Fig. 21 about here.]

Figure 22 shows the comparison between the experimental data obtained by Swanson *et al* [27] and the prediction using LaRC03 [12], Hashin [29] and the proposed criteria.

[Fig. 22 about here.]

For carbon-epoxy IM7/8552 both static and dynamic results are shown in Figure 23. It is observed that the proposed model fits well the experimental results obtained by Koerber *et al* [24] for both static and dynamic cases.

[Fig. 23 about here.]

[Table 4 about here.]

[Table 5 about here.]

5.3 Example 3: Compression and tension of thick unidirectional laminates

Koerber *et al.* [24] presented compression test based on ASTM Standard D 695 of end-loaded thick specimens. The specimens are manufactured using IM7/8552 carbon-epoxy. The material parameters are shown in Table 5.

Two types of test are performed:

- transverse compression;
- off-axis compression at 0°, 15°, 30°, 45°, 60°, 75°.

The test are conducted statically and dynamically. The experimental and predicted relations between the off-axis angle and the peak compressive stress are shown in Figure 24. Good agreement between the experimental results and the model predictions is observed.

[Fig. 24 about here.]

Daniel *et al.* [26] performed off-axis tension and compression on AS4/3501-6 carbon unidirectional laminate. The material properties are shown in Table 4.

Figure 25 shows the predicted relation between the off-axis angle and the ultimate stresses. As before, an excellent agreement is observed.

[Fig. 25 about here.]

5.4 Example 4: σ_{11}-σ_{22} failure envelopes

Hinton *et al.* [10] report biaxial tests of E-Glass/MY750 epoxy lamina. Table 6 shows the material properties of E-Glass/MY750 epoxy.

[Table 6 about here.]

The experimental data and the numerical results are shown in Figure 26. It should be noted that some of the experimental results were affected by experimental errors due to specimen buckling. These points are highlighted in Figure 26. For the other points a good agreement between experiments and the proposed model is observed.

[Fig. 26 about here.]

5.5 Example 5: σ_{11}-τ_{12} failure envelopes

Hinton *et al.* [10] presented experimental test in T300/914C. The relevant mechanical properties of the material are shown in Table 7.

Figure 27 shows the failure envelope generated by the proposed failure criteria and the corresponding experimental data.

The dispersion presented by the data could be an effect of the different angles of the kinking plane. The data shows a high dispersion and some results are clearly affected by experimental errors (as those that present a shear strength higher than S_L^{is}). For this reason, it could be concluded that the comparison between experiments and the proposed model is acceptable.

[Table 7 about here.]

[Fig. 27 about here.]

5.6 Example 6: Influence of hydrostatic pressure

As previously discussed, the proposed model predicts higher strengths when a hydrostatic pressure is applied to the composite material.

However, the prediction of the correct strength under high hydrostatic pressure is a formidable task. In fact, hydrostatic pressure [23] has a very important influence on the mechanical properties of composites:

- the elastic and the shear moduli increase. Depending on the resin used the elastic and shear moduli are linear or bilinear functions of the hydrostatic pressure. The bilinear behavior is considered an effect of the hydrostatic pressure that shifts the sub-zero secondary glass transition temperature;
- some resins exhibit yielding when the applied pressure is greater than 200 MPa. As the yielding phenomenon is pressure-dependent a pressure-dependent yield criterion should be used to predict this behavior. Pae [23] proposed for the resin a criterion that consider the second invariant of the deviatoric stress tensor, J_2, a material constant α_m, and the first invariant of the stress tensor I_1. Successively, this theory was extended to the anisotropic materials.

Hine *et al.* [25] presented experimental results of a E-glass/MY750 lamina tested in compression and in shear under hydrostatic confinement. The material properties are shown in Table 6.

Figures 28(a)-28(b) show the compressive strength and the shear strength as a function of the superimposed hydrostatic pressure of the thick lamina tested under hydrostatic pressure.

[Fig. 28 about here.]

It can be concluded that the proposed criterion can address the increase in the strength of composites under high values of the hidrostatic pressure. However, the correlation between predictions and experimental data appears to be acceptable up to a pressure of 200MPa. It has been argued that this pressure shifts the sub-zero secondary glass temperature at the room temperature at which the test are conducted [23]. At this pressure, the elastic properties change. Since this effect is not accounted for in the model, the experimental data and the predictions differ for hydrostatic pressure higher than 200MPa.

6 Conclusions

Based on the detailed examination of previously proposed failure criteria under several stress states it is concluded that Puck's failure criterion for transverse compression provides accurate predictions of the first ply failure load. However, the prediction of failure of plies embedded in multidirectional laminates requires the use of the in-situ strengths. As a consequence, not only the transverse tensile and shear strengths are in-situ properties: also the compressive transverse strength is an in-situ property that should be calculated as a function of the ply thickness.

It is also concluded that the accuracy of existing three-dimensional failure criteria in the prediction of transverse tensile failure mechanisms depends on relations between the material properties. When using in-situ strengths, these relations are not always satisfied and the failure criteria results in wrong predictions of both the first ply failure load and of the fracture angle. The proposed failure criteria does not have such limitation: the fracture angle is correctly predicted under simple stress states. In addition, a good agreement is observed when comparing the predictions of the proposed failure criteria with experimental data obtained for multi-axial stress states. The predictions of the compressive strength of a composite subjected to high values of hydrostatic pressure is accurate up to values of 200MPa of pressure. For higher values of hydrostatic pressure the quality of the predictions is degraded, which means that the future developments of the model should include the simulation of the effect of the hydrostatic pressure on the elastic properties of the composite material.

While the proposed failure criteria can be used to predict failure envelopes for all conceivable stress states, it is clear that additional experimental work is required to validate the predictions obtained for multi-axial stress states that include out-of-plane components of the stress tensor. Some of the complex stress states analyzed in this paper are clearly not easy to impose experimentally; as an alternative, the suggested additional validation of the proposed criteria for complex stress corresponds to the use of non-linear micro-mechanical finite element models where the complex stress/strain states can be applied using appropriate periodic boundary conditions.

Acknowledgements

The first author would like to acknowledge the support of the Fundação para a Ciência e a Tecnologia under the grant FCT–DFRH–SFRH–BPD–78104–2011.

The second author acknowledges the support of the Fundação para a Ciência

e a Tecnologia under the project PDCT–EME–PME–64984–2006.

References

[1] Tsai, S.W. and Wu, E.M. A General Theory of Strength for Anisotropic Materials, J. Comp. Mater. 1971; 5:58–80.

[2] Christensen, R. M. Stress Based Yield/Failure Criteria for Fiber Composites, Int. J. Solids Structures. 1997; 34:529–543.

[3] Hinton, M.J. and Soden, P.D. Failure criteria for composite laminates, Compos Sci Technol. 1998; 58:1001–1010.

[4] Soden, P.D., Hinton, M.J. and Kaddour, A.S. Lamina properties and lay-up configurations and loading conditions of a range fibre reinforced composite laminates, Compos Sci Technol. 1998; 58:1011–1022.

[5] Puck, A. and Schürmann, H. Failure analysis of frp laminates by means of physically based phenomenological models, Composites Science and Technology. 1998; 58:1045–67.

[6] Sun, C.T. and Tao, J.X. Prediction of failure envelopes and stress strain behaviours of composite laminates, Compos Sci Technol. 1198; 58:1125–1136.

[7] Liu, K.-S and Tsai, S.W. A progressive quadratic failure criterion of a laminate, Compos Sci Technol. 1998; 58:1023–1032.

[8] Kuraishi, A., Tsai, S.W. and Liu, K.K.S. A progressive quadratic failure criterion- part B. Composites Science and Technology. 2002; 62:1683-1695.

[9] Puck, A. and Schürmann, H. Failure analysis of frp laminates by means of physically based phenomenological models, Composites Science and Technology. 2002; 62:1633–62.

[10] Hinton, M.J., Kaddour, A.S. and Soden, P.D. A comparison of the predictive capabilities of current failure theories for composite laminates, judged against experimental evidence, Composites Science and Technology. 2002; 62:1725–97.

[11] Sun, C.T., Tao, J., and Kaddour, A.S. Prediction of failure envelopes and stress-strain behavior of composite laminates, Compos Sci Technol. 2002; 62:1672–1682.

[12] Dávila, C.G., Camanho, P.P. and Rose, C.A. Failure criteria for frp laminates, Journal of Composite Materials. 2005; 39(4):323–345.

[13] Kaddour, A. and Hinton, M. Triaxial failure criteria for polymer composites: part (A) of WWFE-II: comparison between theories, Procedings of the 18th International Conference on Composite Materials, ICCM18, Jeju Island, Korea, August 21-26, 2011.

[14] Maimí, P., Camanho, P.P., Mayugo, J.A. and Dávila, C.G. A continuum damage model for composite laminates: part I - constitutive model. Mechanics of Materials. 2007; 39:897-908.

[15] Maimí, P., Camanho, P.P., Mayugo, J.A. and Dávila, C.G. A continuum damage model for composite laminates: part II - computational implementation and validation. Mechanics of Materials. 2006; 39:909-919.

[16] Puck, A. Calculating the strength of glass fibre/plastic laminates under combined load, Kunstst German Plast. 1969; 55:18–19. Original in German.

[17] Puck, A. and Schneider, W. On failure mechanism and failure criteria of filamentwound glass-fibre/resin composites. Plast Polym. 1969; 33–44. Original in German.

[18] Pinho, S.T., Iannucci, L., and Robinson, P. Physically-based failure models and criteria for laminated fibre-reinforced composites with emphasis on fibre kinking: Part I: Development, Composites Part A. 2006; 37:63–73.

[19] Knops, M. Analysis of Failure in Fiber Polymer Laminates, The Theory of Alfred Puck. Springer, first edition, 2008.

[20] Rosen, V.W. Mechanics of composite strengthening, Metals Park OH: Fiber Composite Materials American Society of Metals. 1965; pages 37–75.

[21] Argon, A.S. Fracture of Composites in: treatise on material science and technology. New york: Academic Press, 1972.

[22] Schultheisz, C.R. and Waas, A.M. Compressive failure of composites. part I. testing and micromechanical theories, Progress in Aerospace Sciences. 1996; 32:1–42.

[23] Pae, K.D. Influence of hydrostatic pressure on the mechanical behavior and properties of unidirectional, laminated, graphite-fibre/epoxy-matrix thick composites, Composites: Part B. 1996; 27B:599–611.

[24] Koerber, H. and Camanho, P.P. High strain rate characterisation of unidirectional carbon-epoxy im7-8552 in transverse compression and in-plane shear using digital image correlation, Mechanics of Materials. 2010; 42:1004–19.

[25] Hine, P.J. The effect of hydrostatic pressure on the mechanical properties of glass fiber/epoxy unidirectional composites, Composites: Part A. 2005; 36:279–89.

[26] Daniel, I.M., Luo, J.J., Schubel, P.M. and Werner, B.T. Interfiber/interlaminar failure of composites under multi-axial states of stress, Composites Science and Technology. 2009; 69:764?-771.

[27] Swanson, S.R., Messick, M.J. and Tian, Z. Failure of carbon/epoxy lamina under combined stress, J. Composite Materials.1987; 21:619–630.

[28] Swanson, S.R. and Qian, Y. Multiaxial characterization of T800/3900-2 carbon/epoxy composites, Composite Science and Technology. 1992; 43:197–203.

[29] Hashin, Z. Failure criteria for unidirectional fibre composites, J. Appl. Mech. 1980; 47:329–34.

[30] Camanho, P.P., Dávila, C.G., Pinho, S.T., Iannucci, L. and Robinson, P. Prediction of in-situ strengths and matrix cracking in composites under transverse tension and in-plane shear, Composites-Part A. 2006; 37:165-176.

[31] Gutkin, R and Pinho, S.T. Practical application of failure models to predict the response of composite structures, Procedings of the 18th International Conference on Composite Materials, ICCM18, Jeju Island, Korea, August 21-26, 2011.

List of Figures

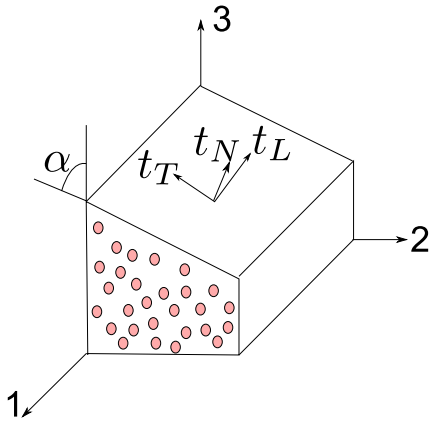

Fig. 1. Components of traction on the fracture plane

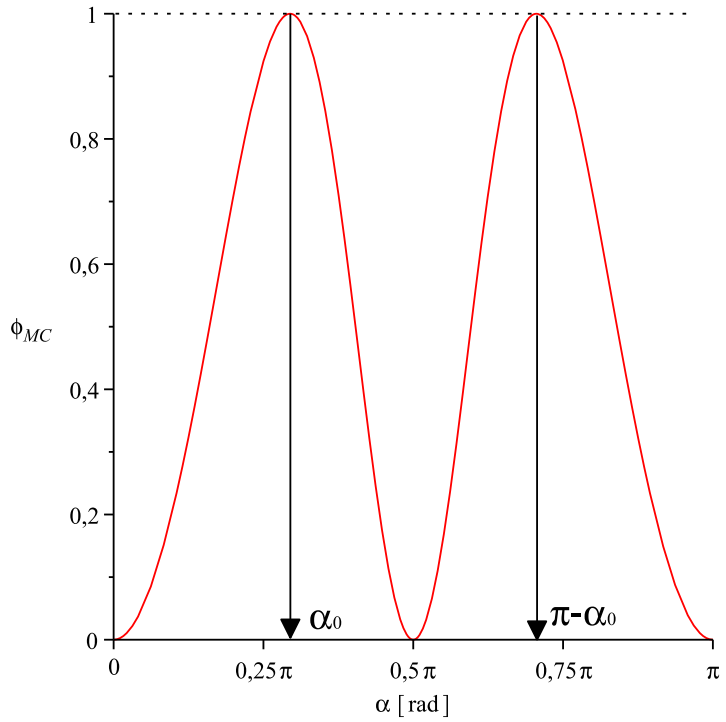

Fig. 2. ϕ_{MC} as a function of α for IM-78552 ($\sigma_{22} = -Y_C^{is}$)

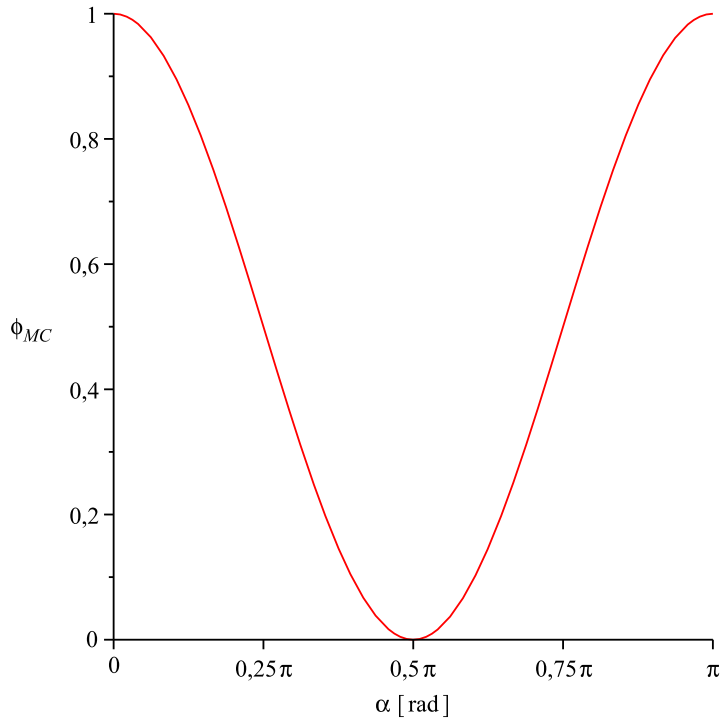

Fig. 3. ϕ_{MC} as a function of α ($\tau_{12} = S_L^{is}$)

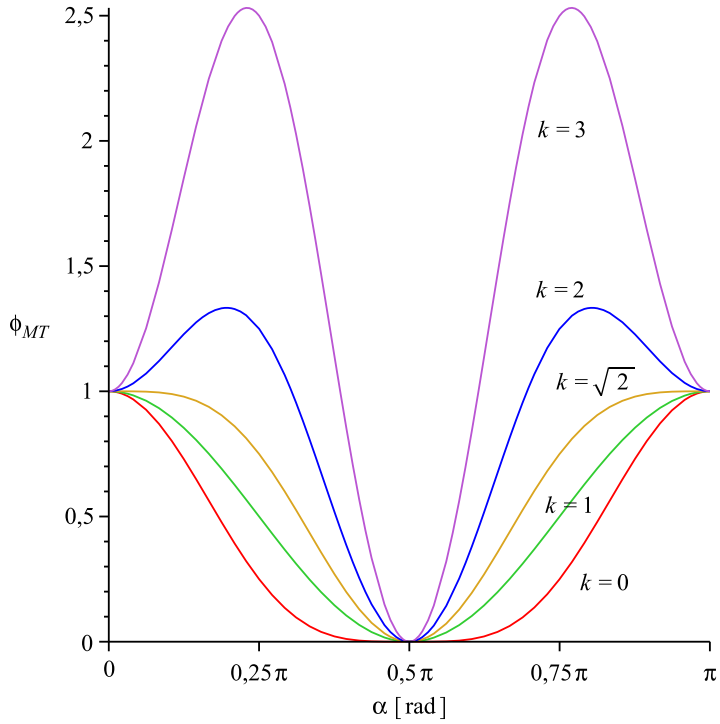

Fig. 4. ϕ_{MT} as a function of α for different values of k ($\sigma_{22} = -Y_T^{is}$)

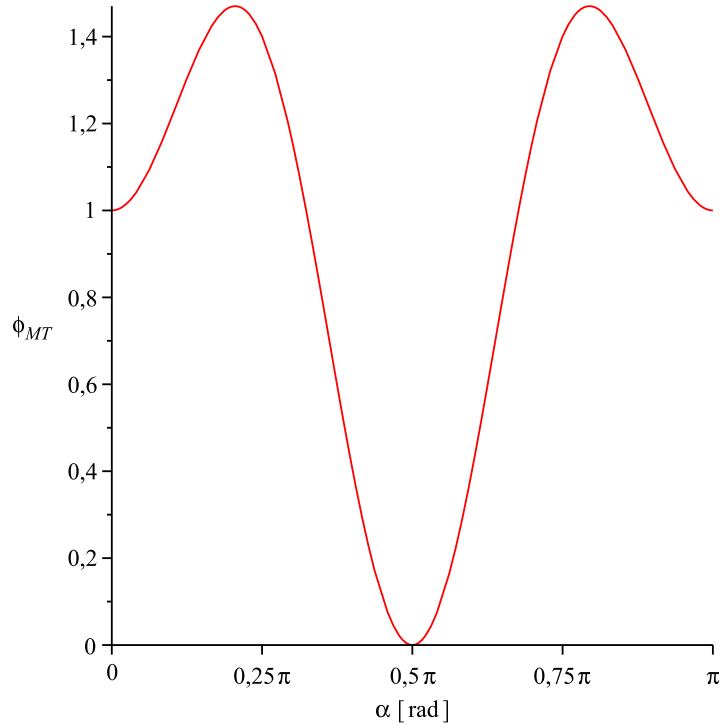

Fig. 5. ϕ_{MT} as a function of α for IM7/8552 (quadratic criterion)

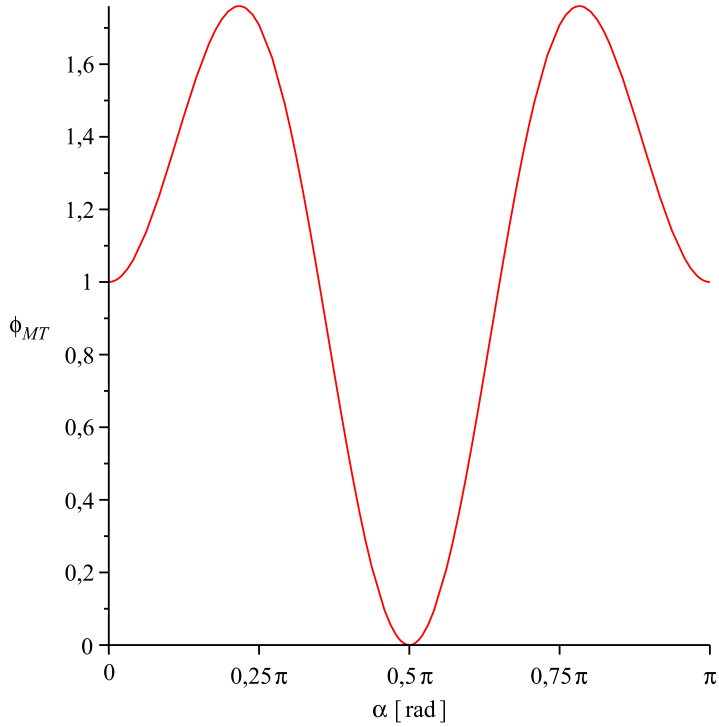

Fig. 6. Puck criterion: ϕ_{MT} as a function of α for IM7/8552 ($\sigma_{22} = Y_T^{is}$)

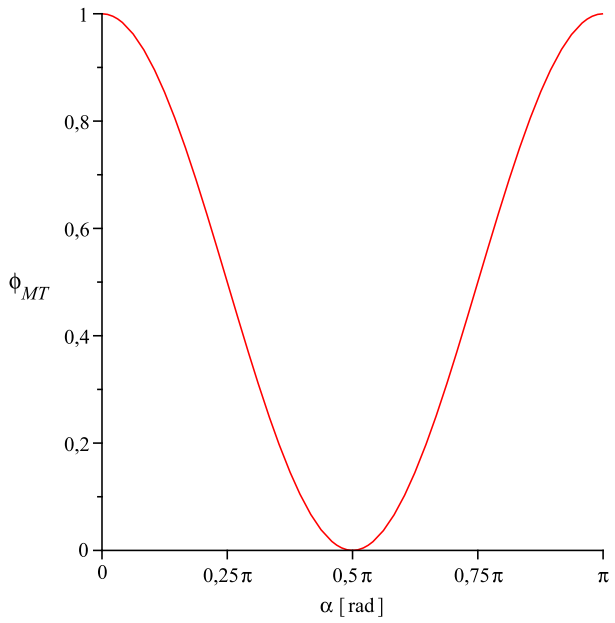

Fig. 7. ϕ_{MT} as a function of α ($\sigma_{22} = Y_T^{is}$)

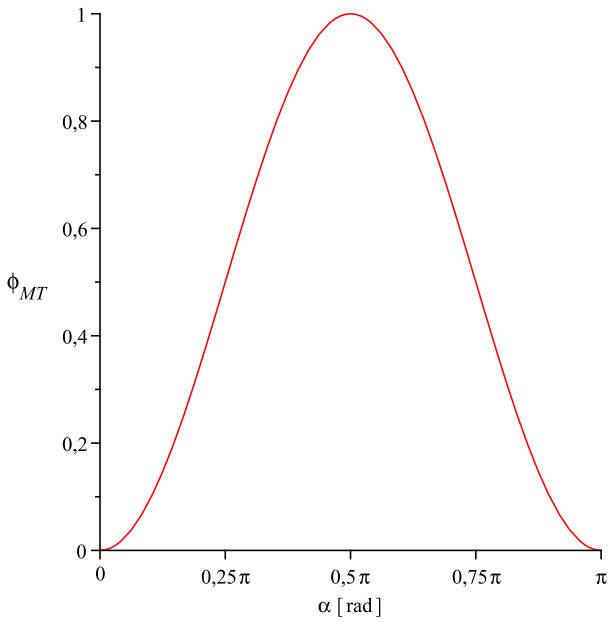

Fig. 8. ϕ_{MT} as a function of α ($\sigma_{33} = Y_T^{is}$)

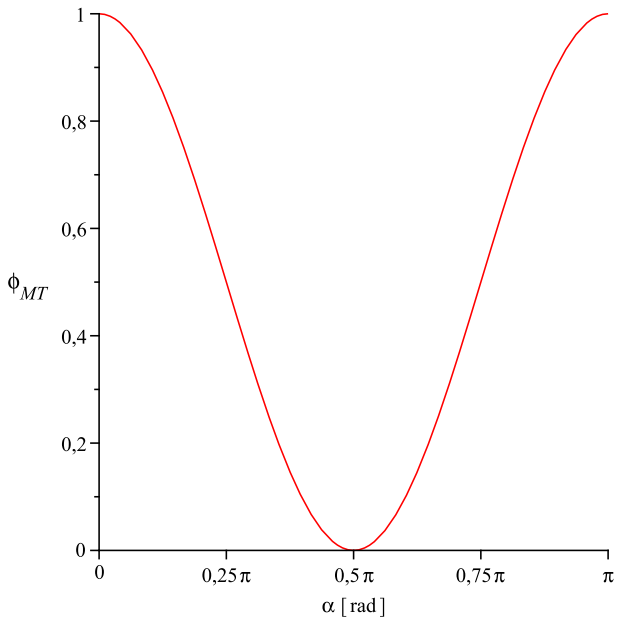

Fig. 9. ϕ_{MT} as a function of α ($\tau_{12} = S_L^{is}$)

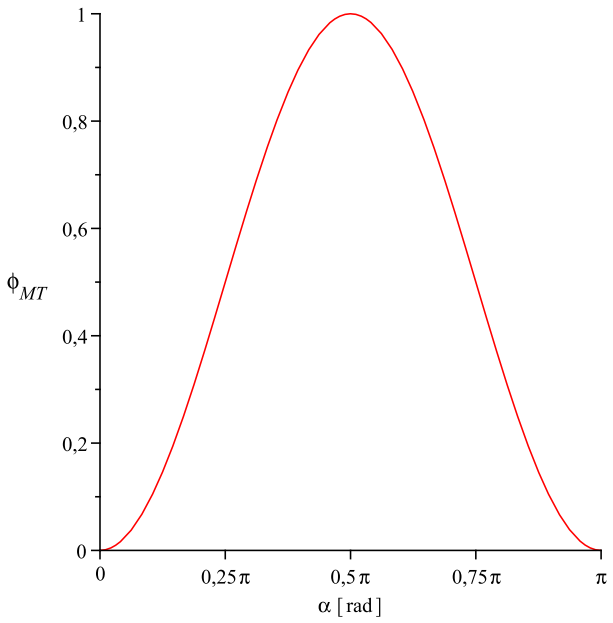

Fig. 10. ϕ_{MT} as a function of α ($\tau_{13} = S_L^{is}$)

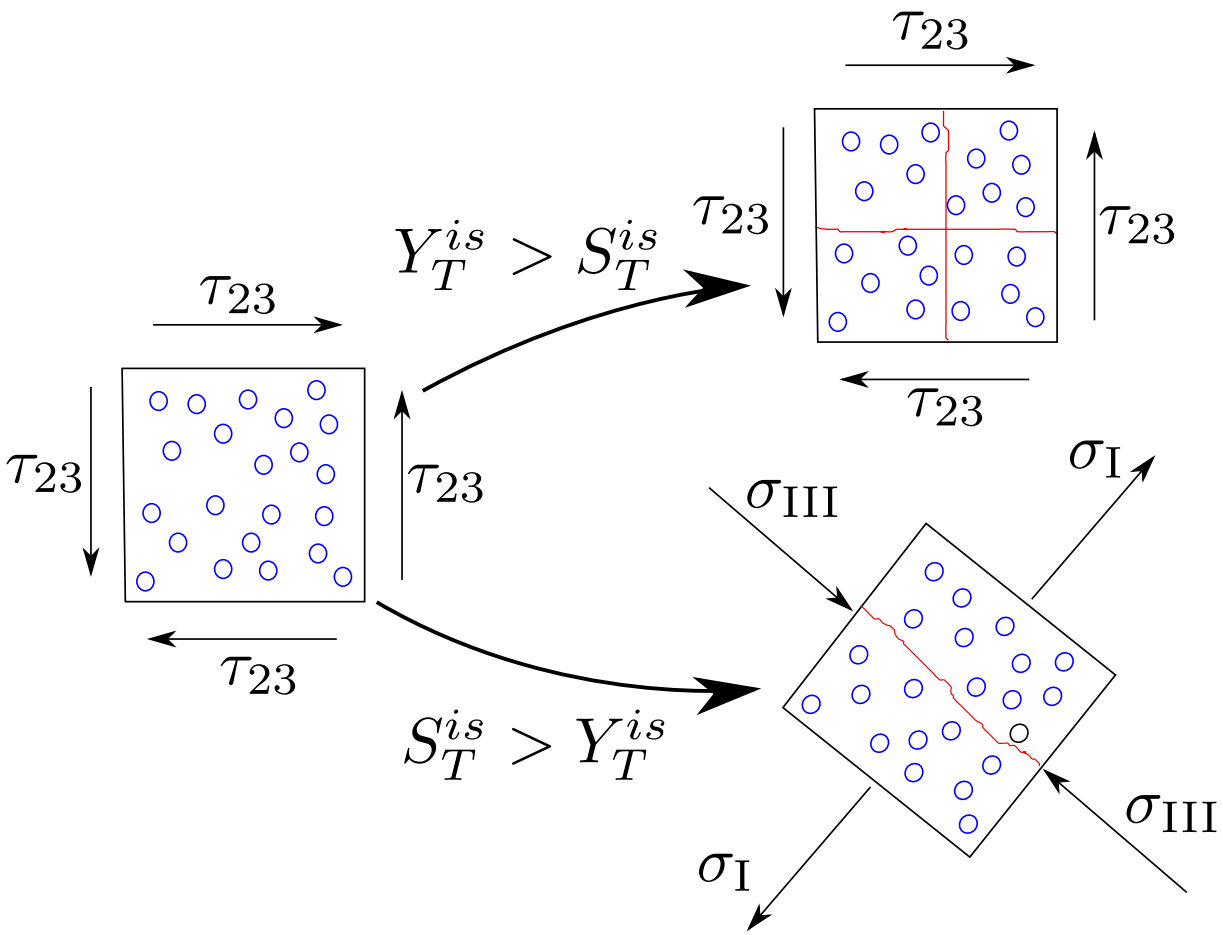

Fig. 11. Transverse shear stress τ_{23} and associated fracture planes.

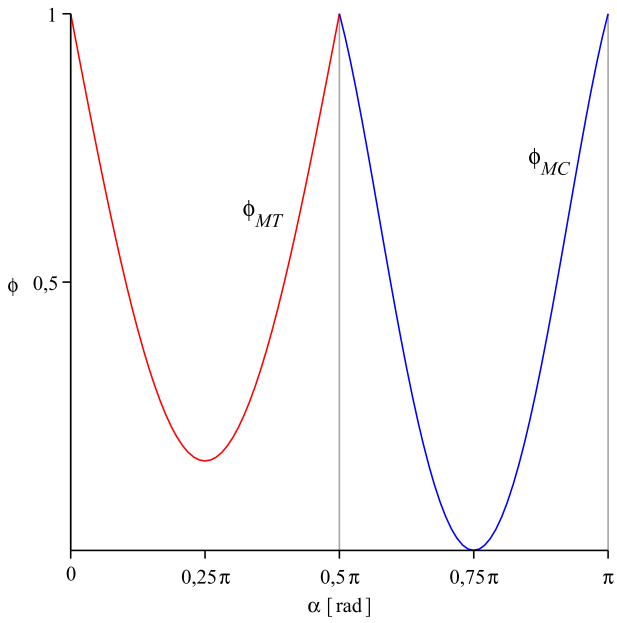

Fig. 12. ϕ_{MT} as a function of α ($\tau_{23} = S_T^{is}$)

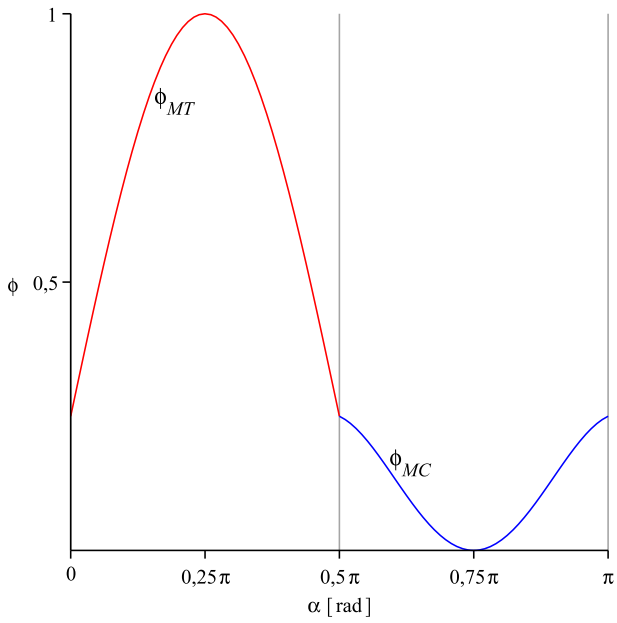

Fig. 13. ϕ_{MT} as a function of α ($\tau_{23} = Y_T^{is}$)

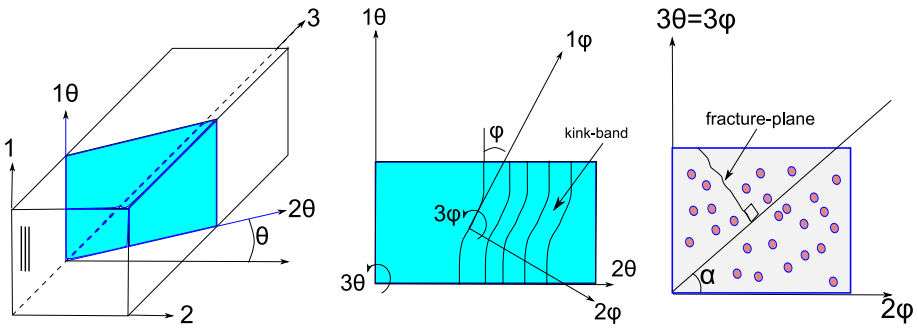

(a) (b) (c)

Fig. 14. Coordinate systems associated to fiber kinking

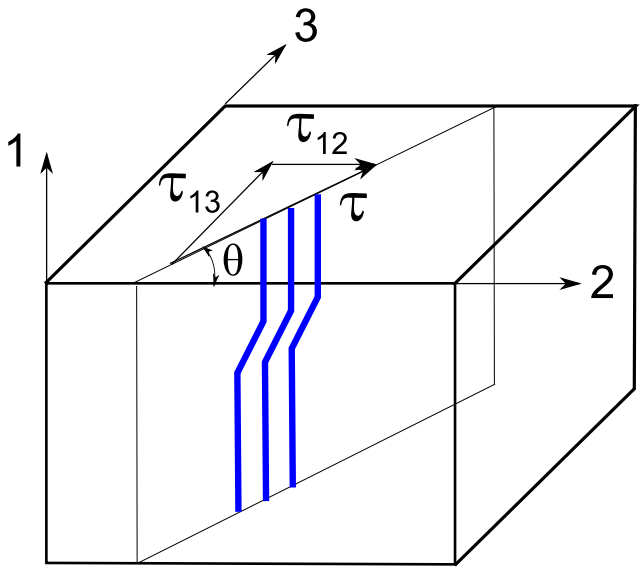

Fig. 15. Kinking plane and involved shear stresses

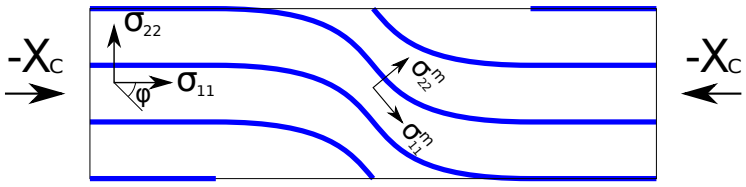

Fig. 16. Stresses in the misalignment frame (2D)

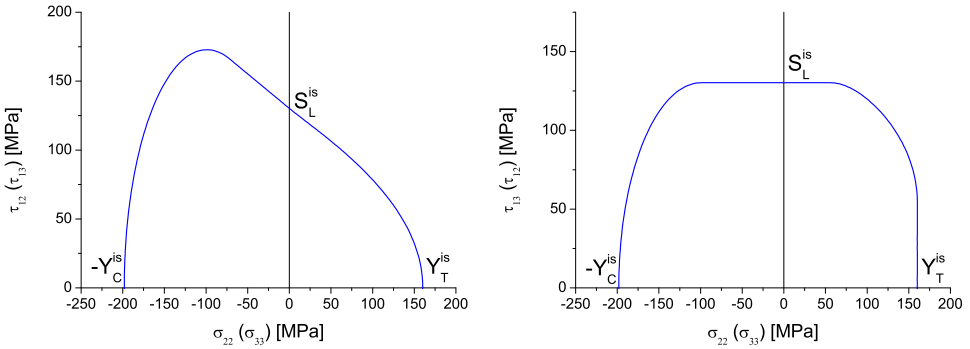

(a) σ_{22}-τ_{12}

(b) σ_{22}-τ_{13}

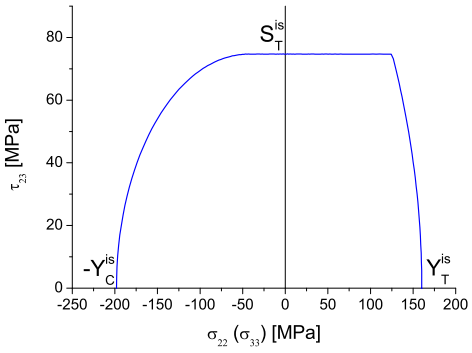

(c) σ_{22}-τ_{23}

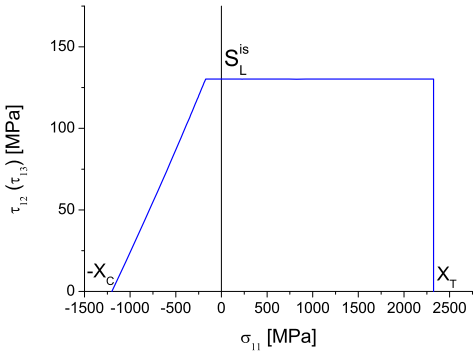

(d) σ_{11}-τ_{12}

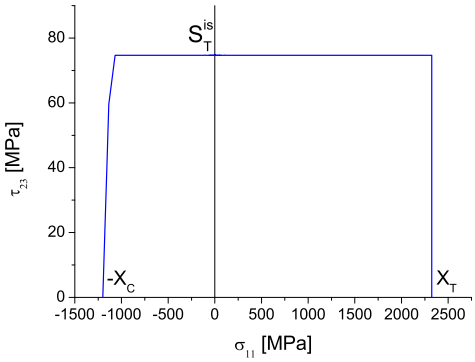

(e) σ_{11}-τ_{23}

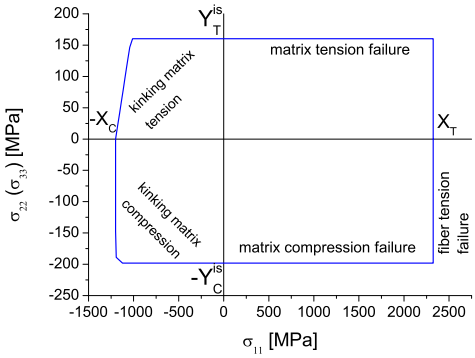

(f) σ_{11}-σ_{22}

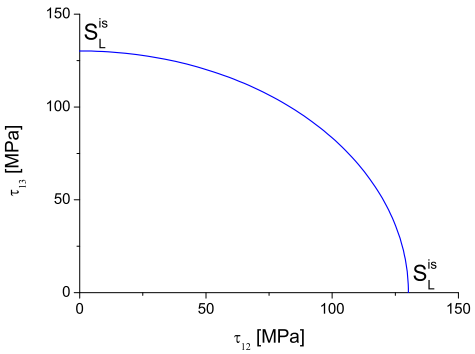

(g) τ_{12}-τ_{13}

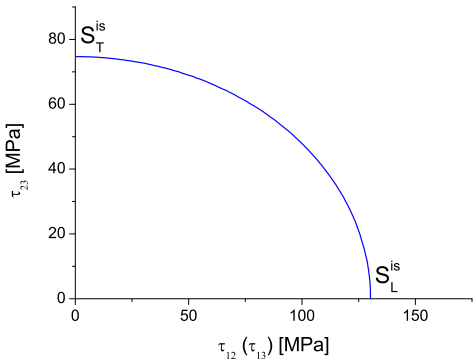

(h) τ_{12}-τ_{23}

Fig. 17. 2D failure envelopes for IM/78552 carbon

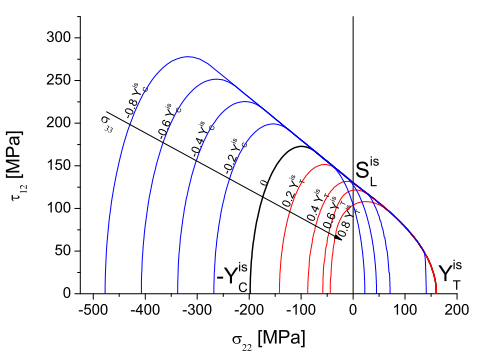

(a) σ_{22}-τ_{12} for different values of σ_{33}

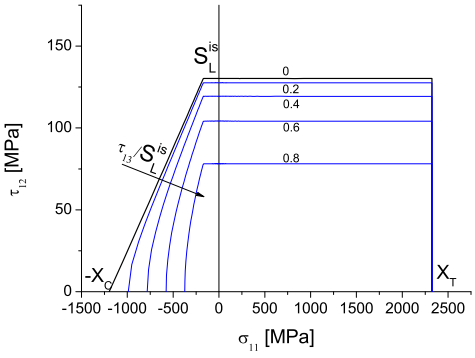

(b) σ_{11}-τ_{12} for different values of τ_{13}

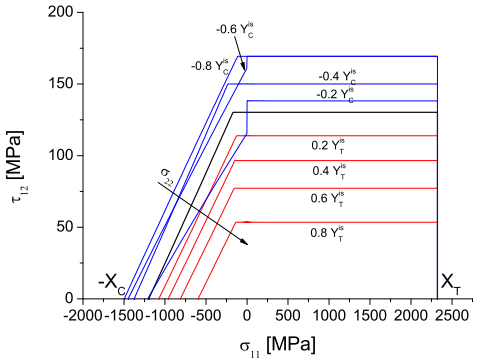

(c) σ_{11}-τ_{12} for different values of σ_{22}

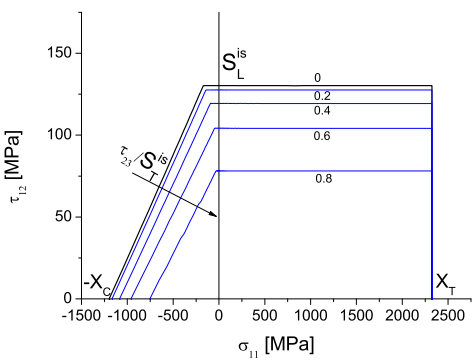

(d) σ_{11}-τ_{12} for different values of τ_{23}

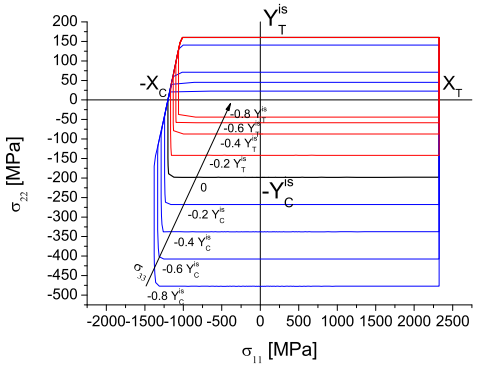

(e) σ_{11}-σ_{22} for different values of σ_{33}

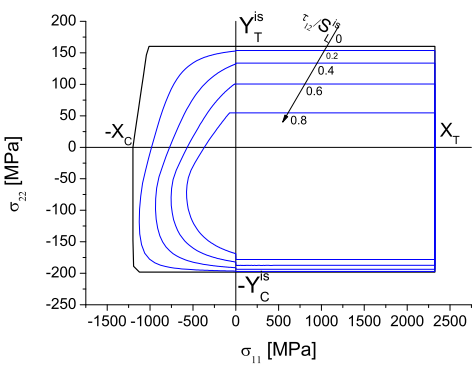

(f) σ_{11}-σ_{22} for different values of τ_{12}

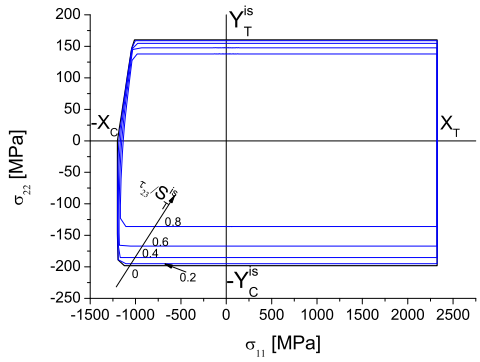

(g) σ_{11}-σ_{22} for different values of τ_{23}

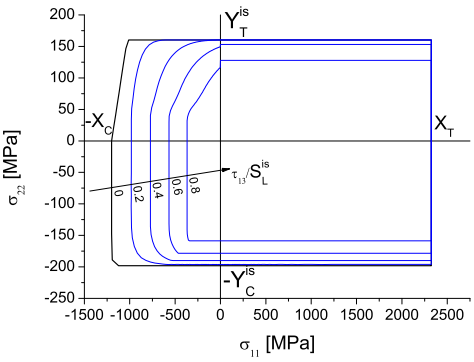

(h) σ_{11}-σ_{22} for different values of τ_{13}

Fig. 18. 3D failure envelopes for IM/78552 carbon

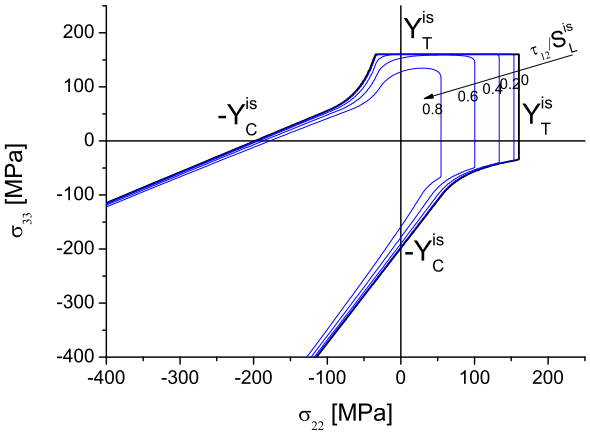

(a) for different values of τ_{12}

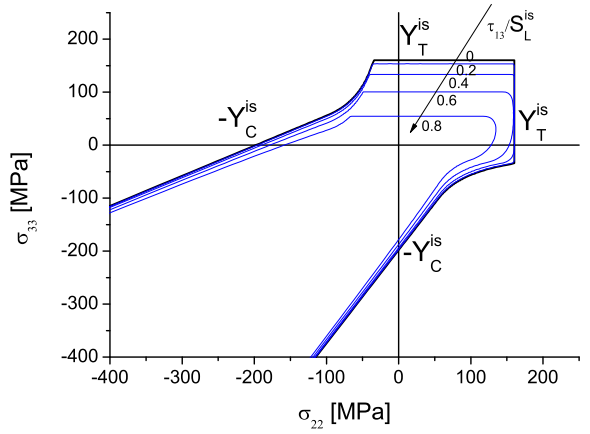

(b) for different values of τ_{13}

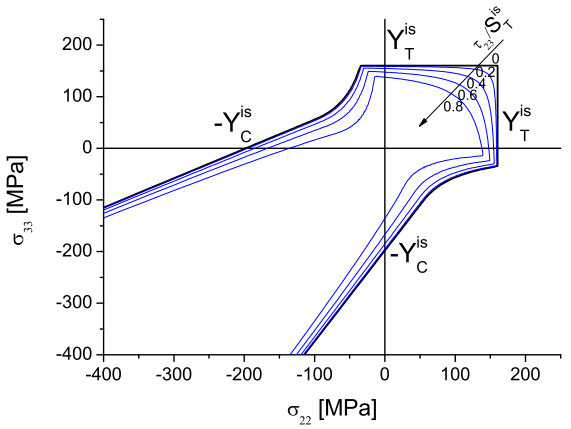

(c) for different values of τ_{23}

Fig. 19. σ_{22}-σ_{33} failure envelopes

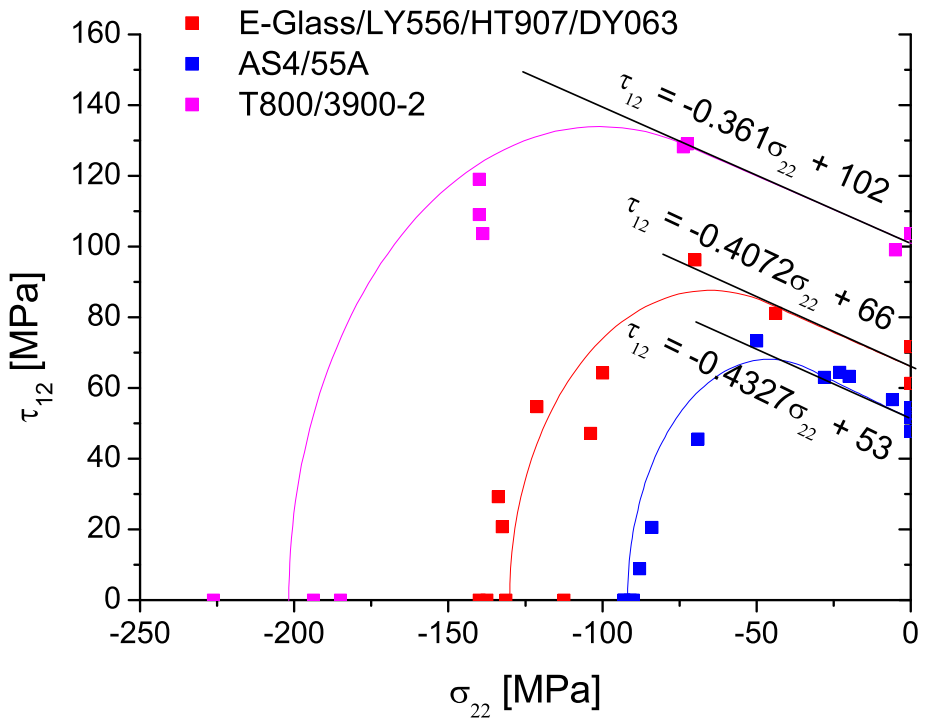

Fig. 20. τ_{12} as a function of σ_{22} for different materials and correspondent values of Y_C^{is}, η_L and S_L^{is} [27,10,28]

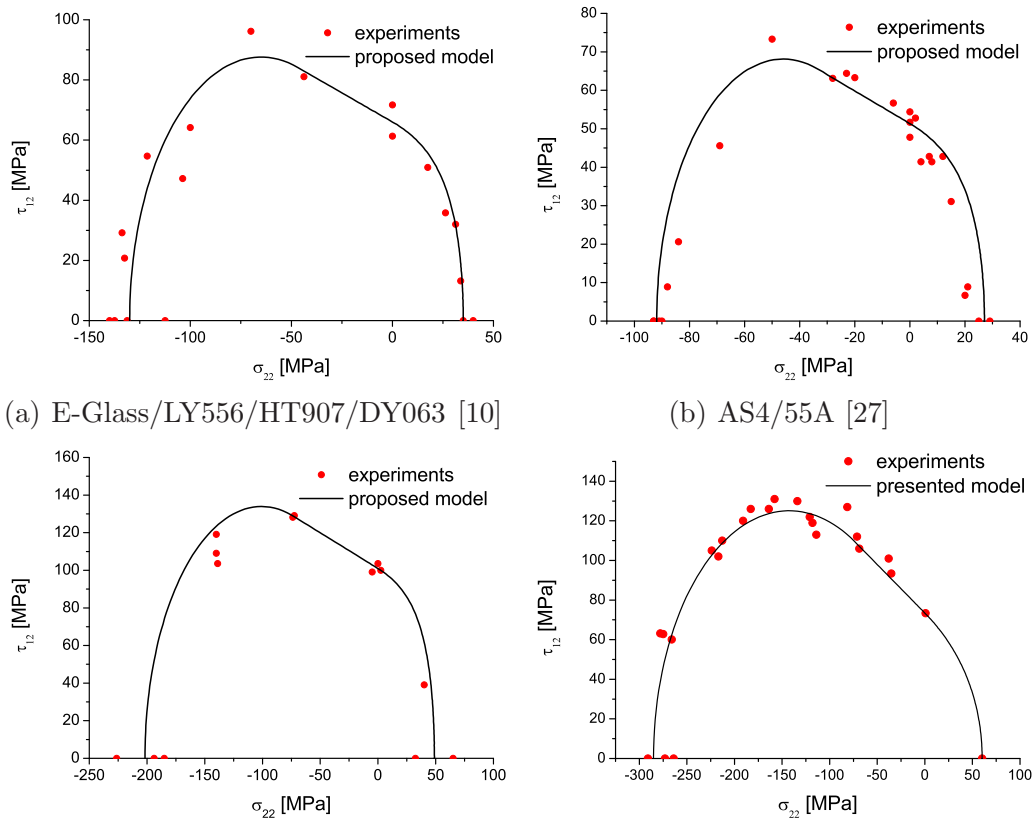

(a) E-Glass/LY556/HT907/DY063 [10] (b) AS4/55A [27]

(c) T800/3900-2 [28] (d) AS4/3501-6 [26]

Fig. 21. σ_{22}-τ_{12} failure envelopes for different materials

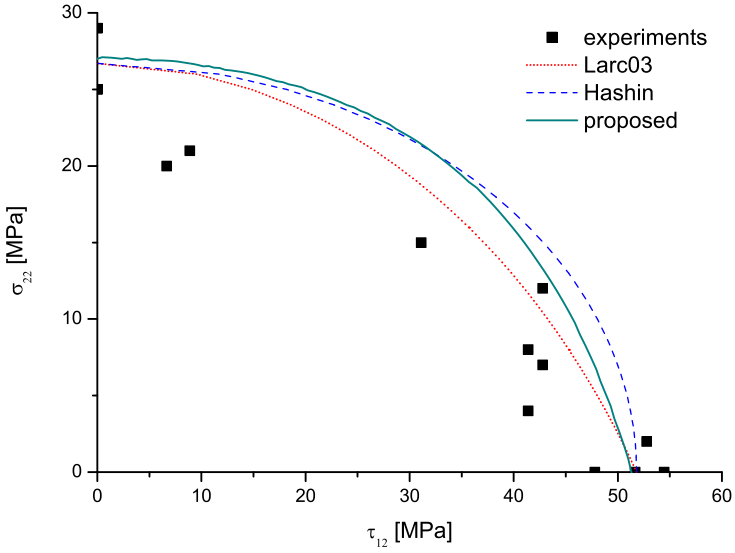

Fig. 22. Comparison between the experimental data obtained in [27] and the predictions using different failure criteria

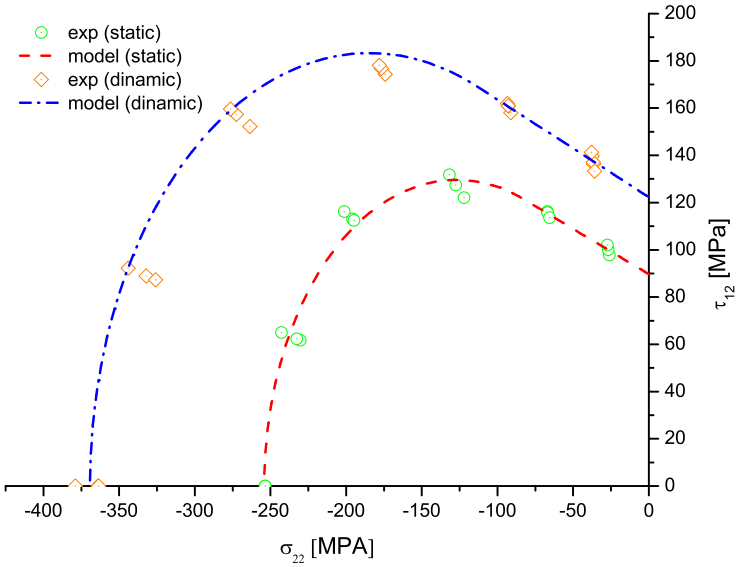

Fig. 23. Static and dynamic test data for IM78552 unidirectional lamina [24]

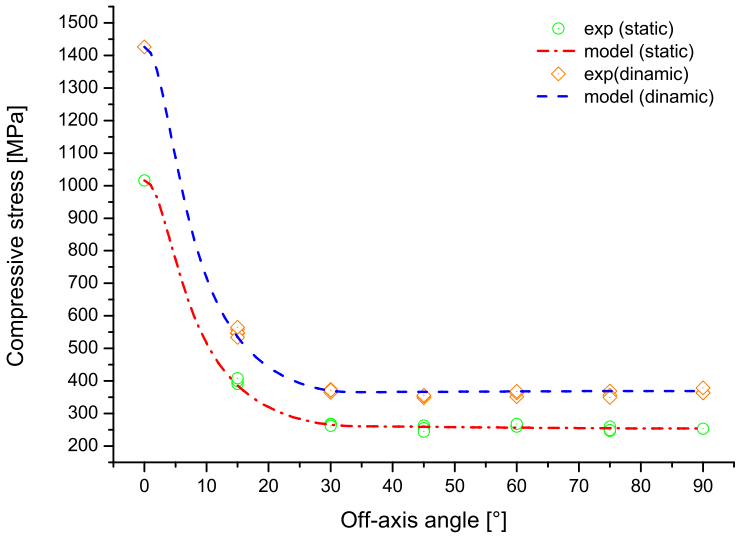

Fig. 24. Off-axis compression test of IM7/8552 carbon lamina [24]

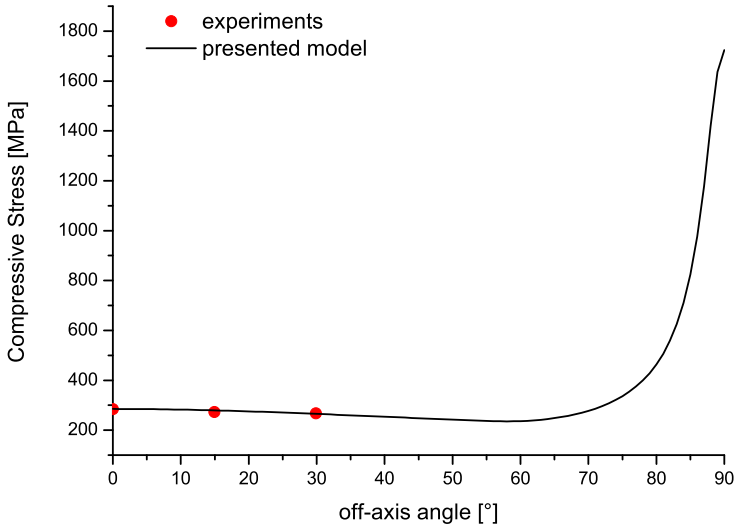

(a) Off-axis tension

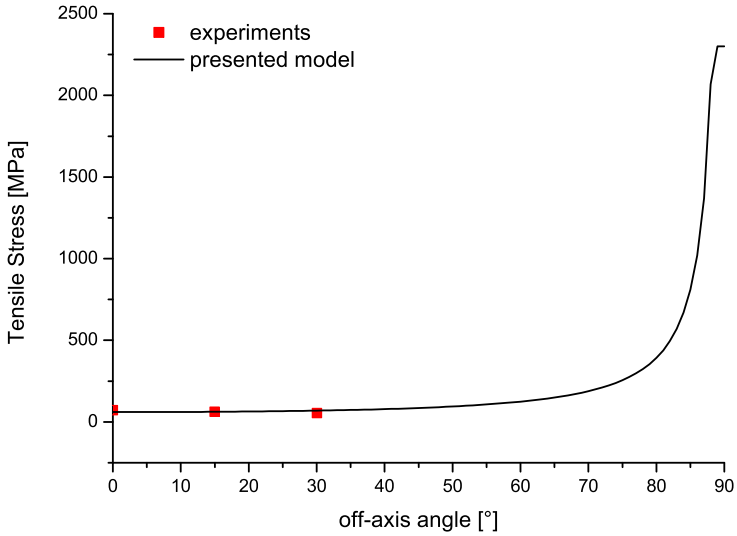

(b) Off-axis compression

Fig. 25. Experimental results for AS4/3501-6 carbon unidirectional lamina [26]

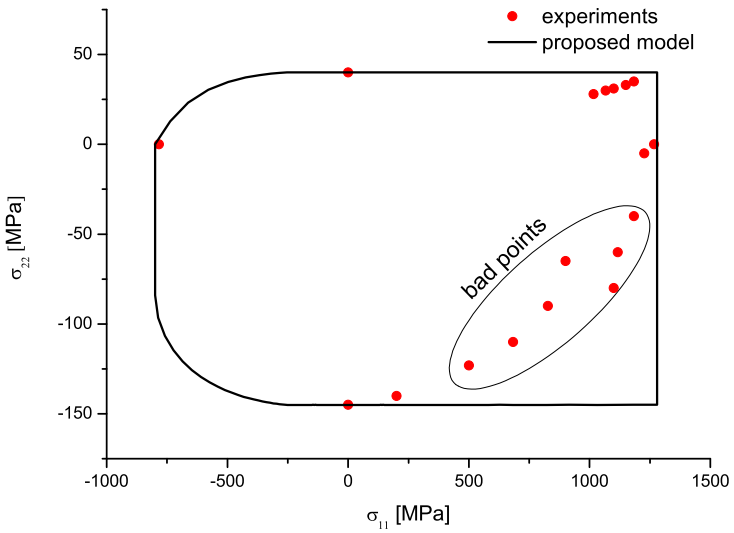

Fig. 26. σ_{11}-σ_{22} failure envelope for E-Glass/MY750 epoxy lamina [10]

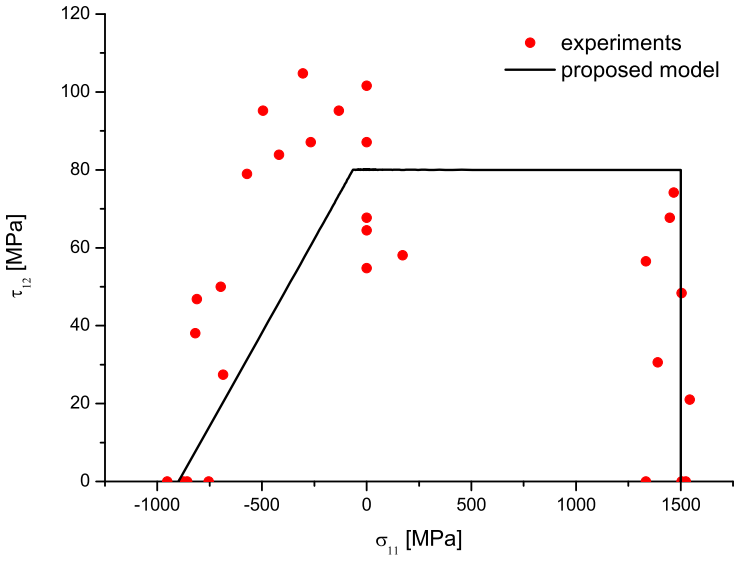

Fig. 27. σ_{11}-τ_{12} failure envelope for T300/914C lamina [10]

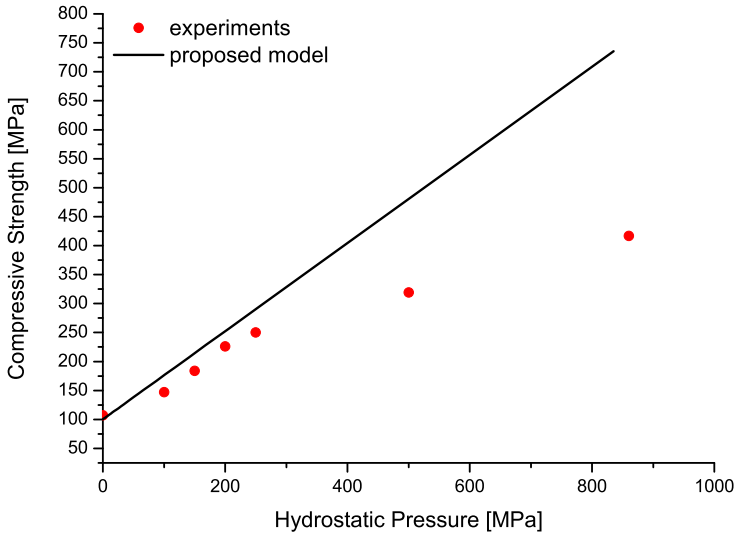

(a) Compressive strength as function of the hydrostatic pressure

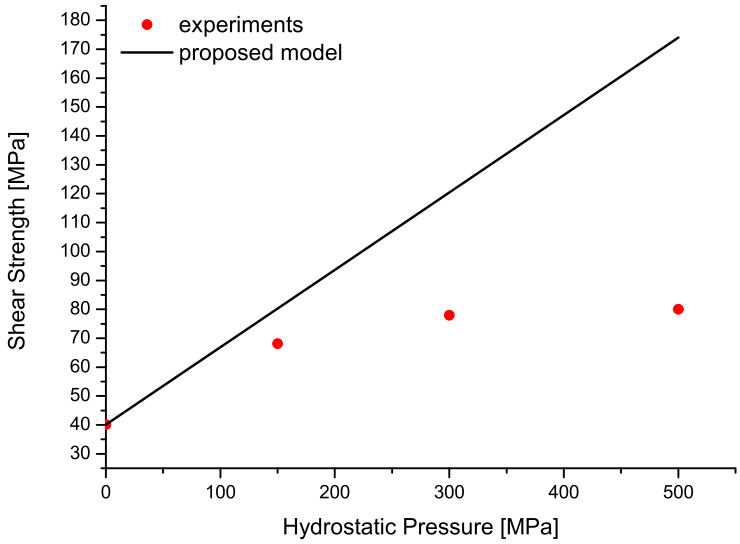

(b) Shear strength as function of the hydrostatic pressure

Fig. 28. Effect of the hydrostatic pressure [25]

List of Tables

X_T	X_C	Y_T^{is}	Y_C^{is}	S_L^{is}	η_L	α_0 (°)
2323.5	1200.1	160.2	198	130.2	0.5	53

Table 1
Mechanical properties of IM7/8552

material	AS4/55A	E-Glass/LY556/HT907/DY063	T800/3900-2
ref.	[27]	[10]	[28]
X_T (MPa)	–	1140	–
X_C (MPa)	–	570	–
Y_T (MPa)	27.0	35	48.8
Y_C (MPa)	91.8	130	201.7
S_L (MPa)	66.0	72	100.9
α_0 (°)	53	53	53

Table 2
Material properties of investigated composites

material	S_L (MPa)	η_L	measured Y_C (MPa)	calculated Y_C (MPa)
AS4/55A	51.3	0.43	91.8	90.2
E-Glass/LY556/HT907/DY063	66.0	0.41	130.0	123.0
T800/3900-2	100.9	0.36	201.7	212.0

Table 3
Material properties of investigated composites

S_L (MPa)	η_L	Y_T (MPa)	X_T (MPa)	X_C (MPa)
73.4	0.49	60.2	2323.5	1200.1

Table 4
Material properties of AS4/3501-6 unidirectional laminate [26]

test type	static	dynamic
X_T (MPa)	2323.5	–
X_C (MPa)	1017.5	1428.0
Y_T (MPa)	160.2	–
S_L (MPa)	89.6	122.3
η_L	0.38	0.41
α_0 (°)	55.3	56.3

Table 5
Material properties of IM78552 [24]

X_T (MPa)	X_C (MPa)	Y_T (MPa)	Y_C (MPa)	S_L (MPa)	α_0 (°)
1280	800	40	145	73	53

Table 6
Material properties of E-Glass/MY750 epoxy [10]

X_T (MPa)	X_C (MPa)	Y_T (MPa)	Y_C (MPa)	S_L (MPa)	α_0 (°)
1500	900	27	200	80	53

Table 7
Material properties of T300/914C [10]